Geophysical Journal International

Geophys. J. Int. (2016) **207,** 481–511
Advance Access publication 2016 July 30
GJI Seismology

doi: 10.1093/gji/ggw287

A no-cost improved velocity–stress staggered-grid finite-difference scheme for modelling seismic wave propagation

Leila Etemadsaeed,[1] Peter Moczo,[2,3] Jozef Kristek,[2,3] Anooshiravan Ansari[4] and Miriam Kristekova[3]

[1]*School of Civil Engineering, College of Engineering, University of Tehran, Tehran, Iran. E-mail: Letemad@ut.ac.ir*
[2]*Faculty of Mathematics, Physics and Informatics, Comenius University Bratislava, Mlynska dolina F1,* 842 48 *Bratislava, Slovakia*
[3]*Earth Science Institute, Slovak Academy of Sciences, Dubravska cesta* 9, 845 28 *Bratislava, Slovakia*
[4]*International Institute of Earthquake Engineering and Seismology (IIEES), Tehran, Iran*

Accepted 2016 July 26. Received 2016 July 26; in original form 2016 February 26

SUMMARY

We investigate the problem of finite-difference approximations of the velocity–stress formulation of the equation of motion and constitutive law on the staggered grid (SG) and collocated grid (CG). For approximating the first spatial and temporal derivatives, we use three approaches: Taylor expansion (TE), dispersion-relation preserving (DRP), and combined TE-DRP. The TE and DRP approaches represent two fundamental extremes. We derive useful formulae for DRP and TE-DRP approximations. We compare accuracy of the numerical wavenumbers and numerical frequencies of the basic TE, DRP and TE-DRP approximations. Based on the developed approximations, we construct and numerically investigate 14 basic TE, DRP and TE-DRP finite-difference schemes on SG and CG. We find that (1) the TE second-order in time, TE fourth-order in space, 2-point in time, 4-point in space SG scheme (that is the standard (2,4) VS SG scheme, say TE-2-4-2-4-SG) is the best scheme (of the 14 investigated) for large fractions of the maximum possible time step, or, in other words, in a homogeneous medium; (2) the TE second-order in time, combined TE-DRP second-order in space, 2-point in time, 4-point in space SG scheme (say TE-DRP-2-2-2-4-SG) is the best scheme for small fractions of the maximum possible time step, or, in other words, in models with large velocity contrasts if uniform spatial grid spacing and time step are used. The practical conclusion is that in computer codes based on standard TE-2-4-2-4-SG, it is enough to redefine the values of the approximation coefficients by those of TE-DRP-2-2-2-4-SG for increasing accuracy of modelling in models with large velocity contrast between rock and sediments.

Key words: Numerical solutions; Numerical approximations and analysis; Computational seismology; Wave propagation.

1 INTRODUCTION

The finite-difference (FD) method is an important tool for numerical modelling in both earthquake and structural seismological investigations (e.g. Robertsson *et al*. 2012; Moczo *et al*. 2014). It is computationally efficient especially for simulating wave propagation and earthquake ground motions in local surface sedimentary structures.

At present, the FD method in seismology means, in fact, a large diverse family of computational schemes and algorithms based on FD approximations of temporal and spatial derivatives, and discrete representation of a medium. Majority of schemes approximate either of the strong forms of the equation of motion and constitutive law—displacement–stress, displacement, displacement–velocity–stress or velocity–stress (VS). The VS formulation is the most used formulation for three main reasons: (1) both the equation of motion and constitutive law (mainly Hooke's law for an elastic or viscoelastic continuum) are the first-order hyperbolic partial differential equations (PDE); (2) it is very naturally FD approximated if a staggered space–time grid is used; (3) particle velocity and stress tensor as field variables are equally suitable for seismic wave propagation, earthquake ground motion and rupture dynamics. These aspects are clearly advantageous. A disadvantage of the VS formulation compared to the displacement–stress and displacement–velocity–stress formulations is larger memory requirements (17/14 times in the elastic case, 20/17 times in the viscoelastic case; see Moczo *et al*. 2001).

Grids. In principle, the VS formulation can be discretized on different space–time grids in order to obtain alternative VS schemes. Four rectangular grids are shown in Fig. 1. The staggered grid (SG) was introduced into seismology by Madariaga (1976) and Virieux (1984, 1986).

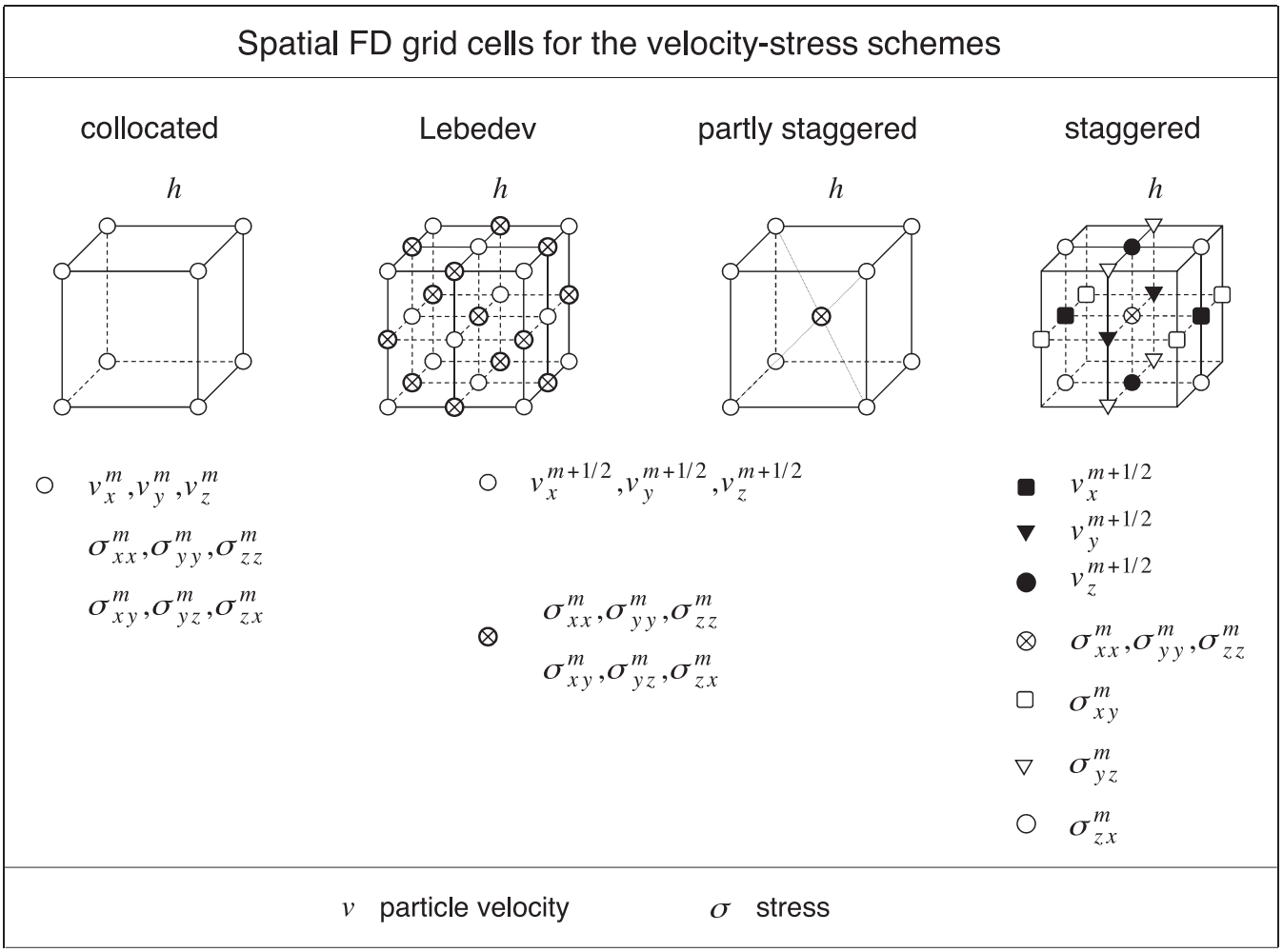

Figure 1. Collocated grid, Lebedev grid, partly staggered grid and staggered grid.

More on the SG FD schemes as well as many references can be found, for example, in Moczo *et al*. (2014). The partly SG was introduced by Andrews (1973), recent elaboration and application can be found, for example, in Saenger *et al*. (2000) and their further publications. The Lebedev (1964) grid was introduced into seismology by Lisitsa (2007) and Lisitsa & Vishnevskiy (2010). The concept of the CG was introduced into seismology probably by Bayliss *et al*. (1986). The CG was recently efficiently used, for example, by Zhang & Chen (2006) and Zhang *et al*. (2012).

In the SG, each of the particle-velocity components as well as each of the shear stress-tensor components has its own spatial grid position whereas the normal stress-tensor components share another grid position. For the second-order approximations of the first derivatives, SG exactly maps structure of the first-order equation of motion and Hooke's law: grid positions of field variables are unambiguously complementary and each variable is located only at a grid position where it is needed for approximating derivatives. This is a key aspect of SG with important consequences. Whereas the staggered spatial distribution of field variables has its clear advantage with respect to approximating derivatives, obviously, it complicates application of boundary conditions or implementation of a constitutive law where different or all components of a field variable (or variables) are needed at one spatial position. The three other types of grids overcome the latter difficulty by partial or complete removal of the staggered distribution.

In the partly SG, all particle-velocity components share a grid position whereas all stress-tensor components share another position located at the centre of a grid cube whose vertices are grid positions of the particle-velocity vector. The consequence is that the first spatial derivative in a coordinate-axis direction is an arithmetic average of four derivatives approximated along the nearest grid lines in the same direction.

In the Lebedev grid, the stress–tensor position is located at the centre of a gridline between two neighbouring grid positions of the particle-velocity vector. Clearly, this is a natural staggered distribution for a general anisotropy.

In the CG, each grid point is a spatial position of both the particle-velocity vector and stress tensor.

One should choose type of grid and scheme that are most appropriate for an investigated problem. Therefore, it is suitable to have such choice available.

Grid dispersion. Due to the temporal and spatial discretization of the equation of motion and constitutive law, the phase and group velocities of a wave simulated in a grid depend on the size of the spatial grid spacing and time step. The grid velocities thus differ from the true velocities in continuum. In other words, dispersion relation of a wave in a grid differs from that in continuum. This phenomenon, known as the grid dispersion, is probably the best known aspect of inaccuracy of FD schemes (for more see, e.g. Holberg 1987; Kindelan *et al*. 1990, and for comparison with local errors see Moczo *et al*. 2014).

In order to have sufficiently accurate numerically simulated wave, it is necessary to reduce (the complete removal is practically impossible) grid dispersion to a level appropriate for an investigated problem. In order to be also computationally efficient, it is necessary to reduce or minimize the number of spatial grid spacings per wavelength that is to be sufficiently accurately propagated, and reduce or minimize the number of arithmetic operations for updating wavefield.

Because the simplest FD schemes (whatever type of grid and approximation) with second-order accuracy in time and space, say (2,2), are significantly inefficient, a variety of approaches for reducing grid dispersion has been developed. We briefly mention some of the optimization approaches.

Optimizations based on Taylor expansion. There are several approaches that use approximations based on Taylor expansion (TE) of temporal and spatial derivatives. The simplest approach is to use a higher-order approximation of spatial derivative. The first such (2,4) VS SG scheme was developed by Levander (1988), later more modellers developed even higher-order (in space) schemes. All these schemes are limited, however, by the second-order accuracy in time.

One possibility to increase also the temporal accuracy was introduced by Lax & Wendroff (1960): higher temporal derivatives in TE of the first temporal derivative are replaced by spatial derivatives through the corresponding equation (equation of motion or constitutive law). Blanch & Robertsson (1997) successfully applied this approach to model wave propagation in viscoelastic medium. Moczo *et al*. (2014) compared the (2,4) VS SG scheme with three alternative (4,4) Lax-Wendroff optimized VS SG schemes. They showed that effect of the optimization is significant for large fractions of the maximum possible time step but all (4,4) schemes degenerate to the (2,4) scheme for a small fraction of the maximum possible time step. The latter is the case of a heterogeneous medium with a large velocity contrast—usual in models of surface sedimentary basins and valleys. MacCormack (1969, 1971) developed a predictor–corrector alternative to the Lax-Wendroff approach. His approach was introduced to seismology by Bayliss *et al*. (1986).

It is worth mentioning the optimally accurate scheme by Geller & Takeuchi (1995, 1998) although it is not applicable to the SG. Their optimization is based on requiring a truncation error whose leading term is identically equal to zero in the case of normal modes in a homogeneous medium. The scheme is extremely accurate. There is one technical and thus practical difficulty, however: the scheme is implicit. Geller and Takeuchi suggested a predictor-corrector algorithm with the second-order conventional scheme as predictor. This scheme is very inaccurate in medium with a large *P*-wave to *S*-wave speed ratio and corrector is unable to remove the imposed inaccuracy.

Tan & Huang (2014) developed two new VS SG schemes with the fourth-order and sixth-order accuracy in time by including a few off-axial grid points in approximating derivatives. The effect of optimization decreases with decreasing fraction of the maximum possible time step.

Optimizations based on minimization of an integral discretization error. Tam & Webb (1993) introduced concept of dispersion-relation-preserving (DRP) schemes for computational acoustics. They aimed to obtain a FD scheme that has the same or almost the same dispersion relation as the original PDE. Dispersion relation is usually obtained by applying the space and time Fourier transform to the PDE. Consequently, Tam & Webb (1993) approximate the spatial derivative in the following way: The first spatial derivative is approximated by a finite series of weighted functional values at grid positions neighbouring the position at which the derivative is to be approximated. The weights are the coefficients of approximation. Application of the space Fourier transform leads to definition of an effective numerical wavenumber. Coefficients are then determined by minimizing difference between the true and numerical wavenumbers. Coefficients of approximation of the first temporal derivative are determined analogously using an application of time Fourier transform and minimizing difference between the true and effective numerical frequencies.

Hixon (1997) applied the DRP approach to spatial discretization, and the low dispersion and dissipation Runge–Kutta scheme of Hu *et al*. (1996) for the time integration to obtain several high-accuracy MacCormack schemes with the best trade-off between accuracy and computing efficiency. Zhang & Chen (2006) and Zhang *et al*. (2012) successfully applied the scheme in their FD modelling of seismic wave propagation on the collocated curvilinear grids.

Chen *et al*. (2015) used the stencil suggested by Tan & Huang (2014) and determined approximation coefficients by minimizing the residual between the Fourier transform of the FD operator and first-order *k*-space operator of Tabei *et al*. (2002) in the least-square sense (*k* meaning the wavenumber).

Finally, let us also mention two other recent approaches. Song *et al*. (2013) developed a novel FD scheme based on the lowrank approximation of the mixed-domain space-wavenumber propagator. Liang *et al*. (2015) suggested satisfying the dispersion relation for a number of uniformly distributed wavenumber points within a wavenumber range with the upper limit determined by the maximum source frequency, the grid spacing and the wave velocity.

As far as we know, the two basic approaches to approximating spatial and temporal derivatives, that is the TE and DRP approach have not been systematically analysed and compared. We consider the SG and CG. Of the four previously mentioned types of grids, the SG and CG may be considered extreme cases in terms of distribution of field variables and approximation of derivatives. We derive DRP FD approximations for the two grids. We investigate the trade-off between the order of approximation and DRP, and the effect of the two aspects on accuracy of

simulating wave propagation. We compare TE, DRP and TE-DRP schemes for their accuracy. For the basic analysis and comparisons, we restrict to the 1-D problem. After we identify two best approximations, we extend the analysis and comparison for the 3-D problem.

2 PROBLEM FORMULATION

The equation of motion and Hooke's law (the stress-strain relation) together with the initial and boundary conditions fully describe a problem of elastic wave propagation. Consider a Cartesian coordinate system with spatial coordinates (x, y, z) or, interchangeably, (x_1, x_2, x_3). Let $\rho(x_i)$; $i \in \{1, 2, 3\}$ be density, $\lambda(x_i)$ and $\mu(x_i)$ Lamé's elastic coefficients, t time, $\vec{v}(x_i, t)$ particle-velocity vector, $\vec{f}(x_i, t)$ body-force per unit volume, and $\sigma_{ij}(x_k, t)$; $i, j, k \in \{1, 2, 3\}$ stress tensor. The equations of motion and Hooke's law in the VS formulation are

$$\rho \frac{\partial v_i}{\partial t} = \frac{\partial \sigma_{ij}}{\partial x_j} + f_i,$$

$$\frac{\partial \sigma_{ij}}{\partial t} = \lambda \frac{\partial v_k}{\partial x_k} \delta_{ij} + \mu \left(\frac{\partial v_i}{\partial x_j} + \frac{\partial v_j}{\partial x_i} \right). \tag{1}$$

Einstein's summation rule over a repeating index is assumed in eq. (1). It is not used, however, in the rest of the article.

The equations simplify in the 1-D problem. For a plane wave propagating in the x-direction they are

$$\rho \frac{\partial v}{\partial t} = \frac{\partial \sigma}{\partial x} + f,$$

$$\frac{\partial \sigma}{\partial t} = C \frac{\partial v}{\partial x}, \tag{2}$$

where either $v(x, t)$ is the x-component of the particle velocity, $\sigma(x, t)$ is the xx-component of the stress tensor, $f(x, t)$ is the x-component of the body force, and $C(x) = \lambda(x) + 2\mu(x)$ in the case of P wave, or $v(x, t)$ is the y- or z-component of the particle velocity, $\sigma(x, t)$ is the xy- or xz-component of the stress tensor, $f(x, t)$ is the y- or z-component of the body force, and $C(x) = \mu(x)$ in the case of the *SH* or *SV* wave, respectively.

We will consider FD schemes solving the 1-D problem on the CG and SG. Note that the *P*, *SV* and *SH* configurations are numerically identical in 1-D.

3 APPROXIMATIONS OF SPATIAL DERIVATIVES BASED ON TAYLOR EXPANSION AND DRP CRITERION ON THE COLLOCATED GRID

3.1 Approximation of spatial derivatives using Taylor expansion

Let Δx be a grid spacing and I be an integer number. For approximating the first spatial derivative of a field variable f at grid position $x = I\,\Delta x$, we can use values of this variable at grid points at $x \pm j\,\Delta x$; $j = 0, 1, 2, 3, \ldots$. Hence, the approximation of the first spatial derivative may be written as

$$\left(\frac{\partial f}{\partial x} \right)_I \approx \frac{1}{\Delta x} \sum_{j=N}^{M} a_j f_{I+j} \tag{3}$$

or, equivalently,

$$\frac{\partial f}{\partial x}(x) \approx \frac{1}{\Delta x} \sum_{j=N}^{M} a_j\, f\,(x + j\Delta x)\,, \tag{4}$$

where a_j are coefficients of approximation. The number of coefficients a_j in approximation (4) is $M - N + 1$. The coefficients are determined so that the TE of the sum on the right-hand side (r.h.s.) of eq. (4) eliminates all derivatives except the first derivative of function $f(x)$. Considering the TE of $f(x + j\Delta x)$,

$$f(x + j\Delta x) = f(x) + \frac{\partial f(x)}{\partial x} \frac{j\Delta x}{1!} + \frac{\partial^2 f(x)}{\partial x^2} \frac{(j\Delta x)^2}{2!} + \cdots, \tag{5}$$

the following system of equations should be satisfied:

$$\sum_{j=N}^{M} j^r\, a_j = \delta_{1r} \quad r = 0, \ldots, M - N. \tag{6}$$

Here, δ_{1r} is the Kronecker delta. Coefficients a_j are obtained straightforwardly by solving system (6). Approximation (4) is accurate up to order $(\Delta x)^{\text{order}}$ where order $= M - N$.

3.2 Approximation of spatial derivatives using DRP criterion

Recall the DRP approach by Tam & Webb (1993). In approximating spatial derivative, Tam and Webb determine coefficients so that the numerical wavenumber be as close as possible to the wavenumber of the true waves. The numerical wavenumber can be obtained using spatial Fourier transform

$$\tilde{f}(k) = \frac{1}{2\pi} \int_{-\infty}^{+\infty} f(x)\, e^{-\mathrm{i}\, k\, x}\, \mathrm{d}x \tag{7}$$

where i denotes the imaginary unit. By applying the Fourier transform to relation (4) we obtain

$$\mathrm{i}k\tilde{f} \approx \left(\frac{1}{\Delta x} \sum_{j=N}^{M} a_j\, e^{\mathrm{i}\, jk\, \Delta x} \right) \tilde{f}. \tag{8}$$

We can see that the expression in parentheses in relation (8) has the meaning of $\mathrm{i}\tilde{k}$ and $\tilde{k}$ may be defined as the numerical wavenumber in approximation (4):

$$\tilde{k} = \frac{-\mathrm{i}}{\Delta x} \sum_{j=N}^{M} a_j e^{\mathrm{i}\, j\, k\, \Delta x}. \tag{9}$$

Define the following L^2-norm error between $k\,\Delta x$ and $\tilde{k}\,\Delta x$ in a desired range $[A, B]$:

$$E \equiv \int_A^B \left\| k\,\Delta x - \tilde{k}\,\Delta x \right\|^2 \mathrm{d}\,(k\,\Delta x)\,. \tag{10}$$

Here, $\|\|$ denotes norm, k is equal to $2\pi/\lambda$, where λ is the wavelength, and $k\,\Delta x = 2\pi/N_\lambda$ with $N_\lambda = \lambda/\Delta x$ being a spatial sampling ratio. Consequently, A and B are dimensionless numbers, inversely proportional to N_λ, specifying the range in which the $\tilde{k}$ should be as close as possible to k. Although we can choose A and B arbitrarily, it is reasonable to determine them according to the minimum wavelength. The smaller the range, the closer are coefficients to the coefficients obtained using TE. Considering, for example, wavelengths longer than $4\Delta x$, $\lambda_{\min} = 4\Delta x = 2\pi/k_{\max}$. Consequently $|k_{\max}\Delta x| = \pi/2$ and $A = -B = -\pi/2$. Let us note that we consider a general range $[A, B]$ in eq. (10) which is different from Tam & Webb (1993) who used $[-\pi/2, \pi/2]$.

We want to find coefficients that would minimize error E. Therefore, we consider condition

$$\frac{\partial E}{\partial a_j} = 0 \quad j = N, \ldots, M. \tag{11}$$

Rewrite the error (10)

$$\begin{aligned} E &= \int_A^B \left\{ \left(\mathrm{Re}\left[k\Delta x - \tilde{k}\,\Delta x\right]\right)^2 + \left(\mathrm{Im}\left[k\Delta x - \tilde{k}\,\Delta x\right]\right)^2 \right\} \mathrm{d}(k\Delta x) \\ &= \int_A^B \left\{ \left(\mathrm{Re}\left[k\,\Delta x + \mathrm{i} \sum_{j=N}^{M} a_j e^{\mathrm{i}jk\Delta x} \right] \right)^2 + \left(\mathrm{Im}\left[k\,\Delta x + \mathrm{i} \sum_{j=N}^{M} a_j e^{\mathrm{i}jk\Delta x} \right] \right)^2 \right\} \mathrm{d}(k\Delta x). \end{aligned} \tag{12}$$

Denote $p \equiv k\Delta x$ and rewrite eq. (12)

$$\begin{aligned} E &= \int_A^B \left\{ \left(\mathrm{Re}\left[p + \mathrm{i} \sum_{j=N}^{M} a_j e^{\mathrm{i}jp} \right] \right)^2 + \left(\mathrm{Im}\left[p + \mathrm{i} \sum_{j=N}^{M} a_j e^{\mathrm{i}jp} \right] \right)^2 \right\} \mathrm{d}p \\ &= \int_A^B \left\{ \left(p - \sum_{j=N}^{M} a_j \sin(jp) \right)^2 + \left(\sum_{j=N}^{M} a_j \cos(jp) \right)^2 \right\} \mathrm{d}p. \end{aligned} \tag{13}$$

Using eq. (13), we can write system of eq. (11) in the form

$$\frac{\partial E}{\partial a_s} = \int_A^B \left\{ -2 \left(p - \sum_{j=N}^{M} a_j \sin(jp) \right) \sin(sp) + 2 \left(\sum_{j=N}^{M} a_j \cos(jp) \right) \cos(sp) \right\} \mathrm{d}p = 0, \quad s = N, \ldots, M. \tag{14}$$

This can be further rearranged as

$$\int_A^B p\sin(sp)\mathrm{d}(p) = \sum_{j=N}^{M}\left\{a_j \int_A^B [\cos(jp)\cos(sp)+\sin(jp)\sin(sp)]\,\mathrm{d}p\right\}$$

$$= \sum_{j=N}^{M}\left\{a_j \int_A^B \cos((j-s)p)\,\mathrm{d}p\right\}. \tag{15}$$

If we define $G_{sj} \equiv \int_A^B \cos((j-s)p)\,\mathrm{d}p$ and $d_s \equiv \int_A^B p\sin(sp)\mathrm{d}p$, system of eq. (15) takes a simple form of a system of linear algebraic equations for unknown coefficients a_j:

$$\sum_{j=N}^{M} G_{sj}\,a_j = d_s \quad s = N,\ldots,M. \tag{16}$$

Note that evaluation of the integrals gives simple formulae

$$\begin{cases} G_{sj} = \dfrac{-\sin(A(j-s))+\sin(B(j-s))}{j-s} & j \neq s \\ G_{sj} = B-A & j = s \end{cases}$$

$$\begin{cases} d_s = \dfrac{\sin(Bs)-Bs\ \cos(Bs)}{s^2} - \dfrac{\sin(As)-As\ \cos(As)}{s^2} & s \neq 0 \\ d_s = 0 & s = 0. \end{cases} \tag{17}$$

3.3 Combination of the DRP criterion and Taylor expansion

By minimizing error (10) we do not ensure consistency of approximation that we quantify by the order of approximation in the standard TE approach. For ensuring such a consistency, it is possible to combine the DRP criterion with the traditional TE approach. We can choose *NFP* coefficients, say free parameters, to satisfy eq. (11), and consequently eq. (16), in order to minimize error (10). Hence, eq. (6) should be satisfied for $r = 0,\ldots,M-N-NFP$. The all coefficients are thus determined by solving one system of equations that is a combination of eq. (16) for $s =$ subscripts of free parameters and eq. (6) for $r = 0,\ldots,M-N-NFP$. Due to the choice of *NFP* free parameters the order of accuracy decreases to $M-N-NFP$.

Consider, for example, $N=-2$, $M=3$, $A=-\pi/2$, $B=\pi/2$, and approximation (4) accurate to order $(\Delta x)^3$. This means $NFP=2$, that is, eq. (16) should be satisfied for two coefficients as free parameters. If we choose a_{-2} and a_2, we require $\partial E/\partial a_{-2}=0$ and $\partial E/\partial a_2=0$. Hence, eq. (6) should be satisfied for $r=0,\ldots,3$ and eq. (16) for $s=-2,\ 2$. We obtain

$$a_{-2}=0.07453,\quad a_{-1}=-0.58514,\quad a_0=-0.23809,$$

$$a_1=0.97979,\quad a_2=-0.27741,\quad a_3=0.04632. \tag{18}$$

Appendix A illustrates details of calculating these coefficients.

Consider now symmetric free parameters and $M=-N$. The number of coefficients is $M-N+1$, eq. (6) should be satisfied for $r=0,\ldots,M-N-NFP$ and the order of accuracy is $M-N-NFP$. Let us include a_0 as a free parameter; this is possible because a_0 is located at the centre and thus does not contradict the symmetry. Eq. (6) still should be satisfied for $r=0,\ldots,M-N-NFP$. However, eq. (6) is automatically satisfied for $r=M-N+1-NFP$ and consequently the actual order of accuracy is $M-N+1-NFP$. This is because in the case of symmetry, there is no difference between considering a_0 as a free parameter or not. In both situations, a_0 is found equal to zero. In other words, it is meaningless to consider a_0 as a free parameter in the case of symmetry.

In Fig. 2, we show the real part of difference $k\Delta x-\tilde{k}\,\Delta x$ as a function of $k\Delta x$ for four collocated-grid approximations: S-TE-2-3-CG—TE second-order 3-point ($N=-1,\ M=1$), S-TE-4-5-CG—TE fourth-order 5-point ($N=-2,\ M=2$), S-DRP-0-5-CG—DRP 0th-order 5-point ($N=-2,\ M=2$) and S-TE-DRP-2-5-(-1,1)-CG—combined TE and DRP second-order 5-point ($N=-2,\ M=2$) with coefficients a_{-1} and a_1 calculated as free parameters. In DRP approximations, $A=-B=-\pi 2$ is used in the evaluation of error (10). The capital S in our abbreviations refers to the spatial derivative.

As expected, S-TE-4-5-CG behaves better than S-TE-2-3-CG. The TE-DRP variant of the second-order approximation, S-TE-DRP-2-5-(-1,1)-CG, also behaves better than S-TE-2-3-CG. Comparison of S-DRP-0-5-CG and S-TE-DRP-2-5-(-1,1)-CG with S-TE-4-5-CG is more complicated. Due to the uniform convergence of TE approximations both considered TE approximations diverge to the positive values. However, both S-DRP-0-5-CG and S-TE-DRP-2-5-(-1,1)-CG for small values of $k\Delta x$ have oscillations around zero value. This is due to the fact that the DRP approximation is based on minimization of the L_2 error.

The range of $k\Delta x$ with 'acceptably small' values of $k\Delta x-\tilde{k}\,\Delta x$ increases from S-TE-2-3-CG through S-TE-4-5-CG and S-TE-DRP-2-5-(-1,1)-CG and is the largest for S-DRP-0-5-CG. For a fixed number of points, the use of the DRP criterion, as compared to the TE approximation, increases the acceptable range of $k\Delta x$ but decreases the order of approximation.

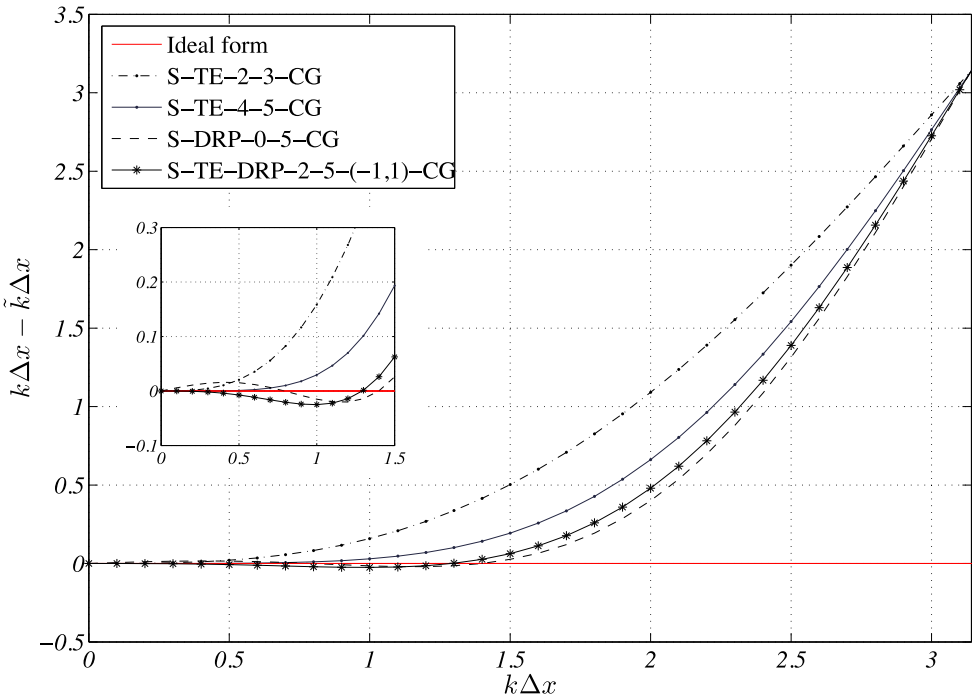

Figure 2. The real part of difference $k\,\Delta x - \tilde{k}\,\Delta x$ as a function of $k\,\Delta x$ for four collocated-grid approximations: S-TE-2-3-CG—TE second-order 3-point ($N = -1,\ M = 1$), S-TE-4-5-CG—TE fourth-order 5-point ($N = -2,\ M = 2$), S-DRP-0-5-CG—DRP 0th-order 5-point ($N = -2,\ M = 2$), S-TE-DRP-2-5-(-1,1)-CG—combined TE and DRP second-order 5-point ($N = -2,\ M = 2$) with coefficients a_{-1} and a_1 calculated as free parameters. In the DRP approximations, $[A, B] = [-\pi/2, \pi/2]$.

3.4 Centred and non-centred collocated-grid approximations

If $M \neq -N$, $\tilde{k}$ is complex. The imaginary part of $\tilde{k}$ can cause instability. On the other hand, if $M = -N$, a spatial odd-even decoupling may occur. The spatial decoupling is due to the centred approximation of the first spatial derivative on the CGs. We can avoid the spatial odd-even decoupling by using a non-centred approximation. In addition, we can elude the complex $\tilde{k}$ by using the averaging

$$\frac{\partial f}{\partial x}(x) \approx \frac{1}{2}\left[\frac{1}{\Delta x}\sum_{j=N}^{M} a_j\, f\,(x + j\Delta x) + \frac{1}{\Delta x}\sum_{j=-M}^{-N} a_j\, f\,(x + j\Delta x)\right]. \tag{19}$$

In this case, the imaginary part of $\tilde{k}$ in the first term of r.h.s. of eq. (19) is negative of the imaginary part of $\tilde{k}$ in the second term. Hence, if we approximate the first spatial derivative on the CG by eq. (19), the final $\tilde{k}$ is real.

As a consequence, choice of some coefficients as free parameters should not prevent elimination of the imaginary part of $\tilde{k}$. If we choose a_j as a free parameter in the first term of the r.h.s. of eq. (19), we have to choose a_{-j} as a free parameter in the second term.

The elimination of the imaginary part of $\tilde{k}$ is illustrated in Fig. 3. The figure shows the imaginary parts of $\tilde{k}\,\Delta x$ as a function of $k\Delta x$ for four approximations on the CG: S-TE-4-5-CG(1)—TE fourth-order 5-point ($N = -3,\ M = 1$), S-TE-4-5-CG(2)—TE fourth-order 5-point ($N = -1,\ M = 3$), S-TE-DRP-2-5-(-1,1)-CG(1)—combined TE and DRP second-order 5-point ($N = -3,\ M = 1$), and S-TE-DRP-2-5-(-1,1)-CG (2)—combined TE and DRP second-order 5-point ($N = -1,\ M = 3$); the two latter approximations with coefficients a_{-1} and a_1 calculated as free parameters. The imaginary parts of $\tilde{k}\,\Delta x$ for S-TE-4-5-CG(1) and S-TE-DRP-2-5-(-1,1)-CG(1) are negative of the imaginary parts of $\tilde{k}\,\Delta x$ for S-TE-4-5-CG(2) and S-TE-DRP-2-5-(-1,1)-CG(2), respectively. Hence, approximation (19) leads to real $\tilde{k}$.

Let us note that for sufficiently small Δx, there is $k\,\Delta x \leq 1$ and the imaginary parts of $\tilde{k}\,\Delta x$ for the above approximations are close to zero.

3.5 Partial summary

In Section 3, we derived useful formulae for approximating spatial derivatives on the CG based on TE, DRP criterion and combination of the two approaches. We analysed the approximations. We may point out that for a fixed number of points the use of the DRP criterion, as compared to the Taylor-expansion approximation, increases the acceptable range of $k\Delta x$ but decreases the order of approximation. We also investigated the use of centred and non-centred approximation for spatial derivatives.

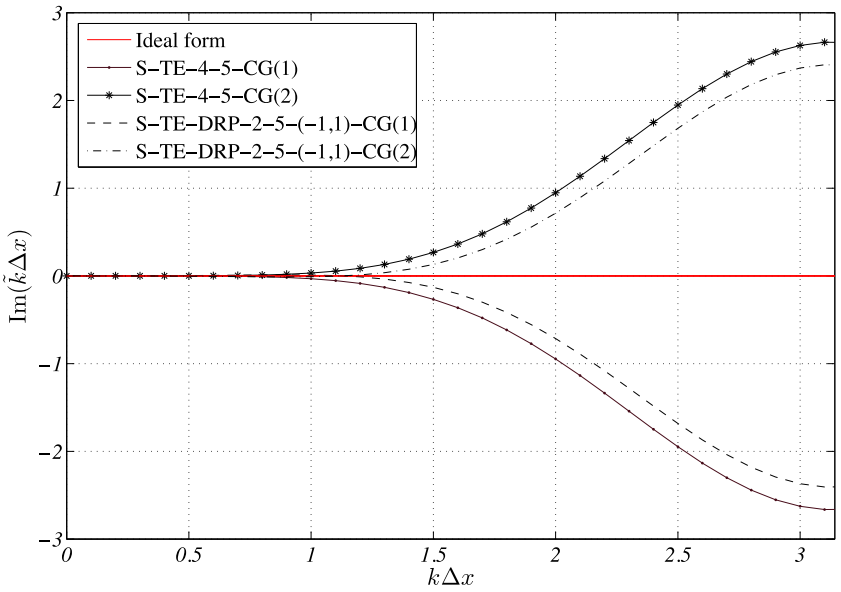

Figure 3. The imaginary parts of $\tilde{k}\,\Delta x$ as a function of $k\,\Delta x$ for four collocated-grid approximations: S-TE-4-5-CG(1)—TE fourth-order 5-point ($N=-3,\ M=1$), S-TE-4-5-CG(2)—TE fourth-order 5-point ($N=-1,\ M=3$), S-TE-DRP-2-5-(-1,1)-CG(1)—combined TE and DRP second-order 5-point ($N=-3,\ M=1$) with coefficients a_{-1} and a_1 calculated as free parameters, and S-TE-DRP-2-5-(-1,1)-CG(2)—combined TE-DRP second-order 5-point ($N=-1,\ M=3$) with coefficients a_{-1} and a_1 calculated as free parameters. In the DRP approximation, $[A,\,B]=[-\pi/2,\,\pi/2]$.

4 APPROXIMATIONS OF TEMPORAL DERIVATIVES BASED ON TAYLOR EXPANSION AND DRP CRITERION ON THE COLLOCATED GRID

For approximating temporal derivative in FD, we can use two different approaches. Let Δt be a time step. We want to approximate the first temporal derivative of a field variable f at a time level m corresponding to time $t=m\Delta t$.

The first approach. We can consider a time marching scheme. If the solution is known until time level m we can use the approximation

$$f^{m+1}-f^{m}\approx\Delta t\sum_{j=0}^{M}\beta_j\left(\frac{\partial f}{\partial t}\right)^{m-j} \tag{20}$$

or, equivalently,

$$f\,(t+\Delta t)-f\,(t)\approx\Delta t\sum_{j=0}^{M}\beta_j\frac{\partial f}{\partial t}\,(t-j\Delta t)\,. \tag{21}$$

The second approach. We can approximate temporal derivative analogously to approximating the spatial derivative:

$$\left(\frac{\partial f}{\partial t}\right)^{m}\approx\frac{1}{\Delta t}\sum_{j=N}^{M=1}b_j\,f^{m+j} \tag{22}$$

or, equivalently,

$$\frac{\partial f}{\partial t}(t)\approx\frac{1}{\Delta t}\sum_{j=N}^{M=1}b_j\,f(t+j\Delta t). \tag{23}$$

Coefficients β_j and b_j are the coefficients of approximations.

Appendix B illustrates how the two approaches can be applied to an equation with the temporal derivative.

4.1 The first approach

4.1.1 Approximation of temporal derivatives using Taylor expansion

Application of the TE to the left-hand side (l.h.s.) of eq. (21) and to the derivative on the r.h.s. of the equation gives, respectively,

$$f\,(t+\Delta t)-f\,(t)=\frac{\Delta t}{1!}\frac{\partial f\,(t)}{\partial t}+\frac{\Delta t^2}{2!}\frac{\partial^2 f\,(t)}{\partial t^2}+\frac{\Delta t^3}{3!}\frac{\partial^3 f\,(t)}{\partial t^3}+\cdots \tag{24}$$

and

$$\frac{\partial f(t-j\Delta t)}{\partial t} = \frac{\partial f(t)}{\partial t} - \frac{j\Delta t}{1!}\frac{\partial^2 f(t)}{\partial t^2} + \frac{(j\Delta t)^2}{2!}\frac{\partial^3 f(t)}{\partial t^3} - \cdots \tag{25}$$

The number of unknown coefficients β_j in approximation (21) is $M+1$. It follows from eqs (21), (24) and (25) that the unknown coefficients β_j have to satisfy the following system of equations:

$$\sum_{j=0}^{M} (-j)^r \beta_j = \frac{r!}{(r+1)!} = \frac{1}{r+1} \quad r = 0, \ldots, M. \tag{26}$$

Coefficients β_j are obtained straightforwardly by solving system (26). Approximation (21) is accurate up to order $(\Delta t)^{\text{order}}$ where order $= M$.

4.1.2 Approximation of temporal derivatives using DRP criterion

In approximating temporal derivative, Tam & Webb (1993) determine coefficients so that the numerical frequency be as close as possible to the frequency of the true waves. We can obtain a numerical frequency using the Holomorphic Fourier transform

$$\hat{f}(\omega) = \frac{1}{2\pi}\int_0^{+\infty} f(t) e^{\mathrm{i}\omega t}\,\mathrm{d}t \tag{27}$$

(Tam and Web called it Laplace transform.) Application of the transform to the l.h.s. and r.h.s. of eq. (21) gives, respectively,

$$\begin{aligned}\text{Holomorphic Fourier}\{f(t+\Delta t) - f(t)\} &= \frac{1}{2\pi}\int_0^{+\infty} [f(t+\Delta t) - f(t)]\, e^{\mathrm{i}\omega t}\mathrm{d}t \\ &= \hat{f}(\omega)\ \left(e^{-\mathrm{i}\omega\Delta t} - 1\right)\end{aligned} \tag{28}$$

and

$$\begin{aligned}\text{Holomorphic Fourier}&\left\{\Delta t \sum_{j=0}^{M} \beta_j \frac{\partial f}{\partial t}(t - j\Delta t)\right\} \\ &= \frac{1}{2\pi}\int_0^{+\infty}\left[\Delta t \sum_{j=0}^{M} \beta_j \frac{\partial f}{\partial t}(t - j\Delta t)\right] e^{\mathrm{i}\omega t}\mathrm{d}t \\ &= -\Delta t\ \mathrm{i}\omega\hat{f}(\omega)\sum_{j=0}^{M}\beta_j e^{\mathrm{i}j\omega\Delta t}.\end{aligned} \tag{29}$$

In the latter equation, we assumed zero initial conditions. The numerical frequency $\tilde{\omega}$ can be defined as

$$\tilde{\omega} = \frac{\mathrm{i}\left(e^{-\mathrm{i}\omega\Delta t} - 1\right)}{\Delta t \sum\limits_{j=0}^{M}\beta_j\, e^{\mathrm{i}j\omega\Delta t}}. \tag{30}$$

As shown by Tam & Webb (1993), the relation between $\tilde{\omega}$ and ω is not one to one; we will illustrate this later. Consequently, the marching scheme (21) will contain spurious numerical solutions.

Tam & Webb (1993) introduced a weighted integral error E_1 for quantifying difference between $\tilde{\omega}$ and ω in the range $[-0.5, 0.5]$:

$$E_1 = \int_{-0.5}^{0.5} \left\{\chi(\mathrm{Re}\,[\omega\Delta t - \tilde{\omega}\Delta t])^2 + (1-\chi)(\mathrm{Im}\,[\omega\Delta t - \tilde{\omega}\Delta t])^2\right\}\mathrm{d}(\omega\Delta t)\,. \tag{31}$$

Here, χ has a role of weighting the degree of emphasis on having better wave propagation characteristics (real part) or damping characteristics (imaginary part). Tam & Webb (1993) used $\chi = 0.36$ as a well-balanced choice. Unknown coefficients β_j in eq. (21) can be found by minimizing E_1:

$$\frac{\partial E_1}{\partial \beta_j} = 0\ ,\ \ j = 0, \ldots, M. \tag{32}$$

Eq. (32) make a system of nonlinear equations. Tam & Webb (1993) solved the system combining the TE and DRP criterion. In such an approach, only one coefficient, say free parameter, is calculated using eq. (32), and eq. (26) should be satisfied for $r = 0, \ldots, M-1$. For example, if M is equal to 3 (Tam and Webb used only $M = 3$), four coefficients have to be determined. Consequently, four equations are

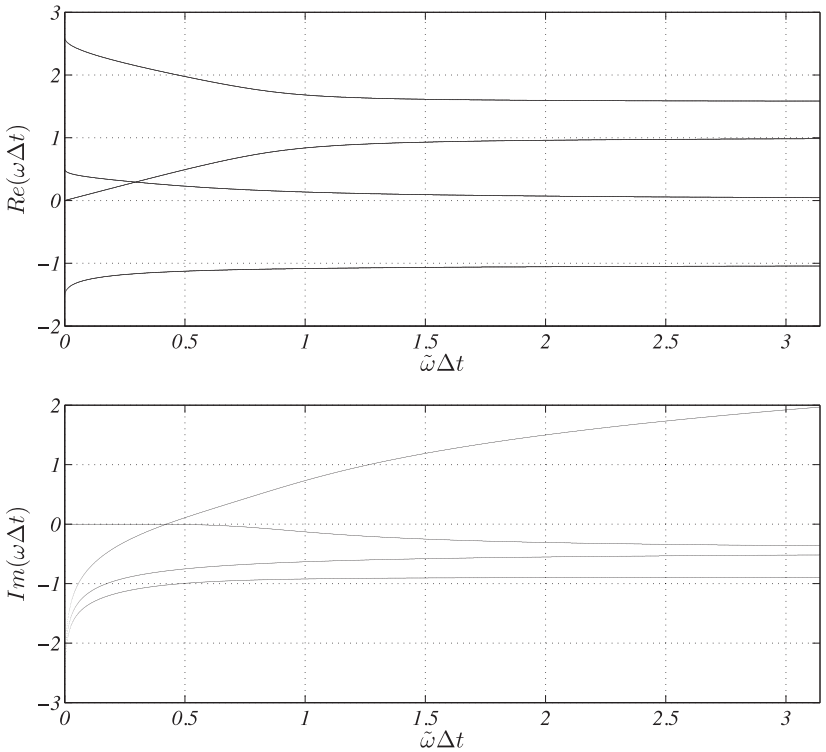

Figure 4. $\omega\,\Delta\,t$ versus $\tilde{\omega}\,\Delta\,t$ for coefficients in eq. (33). The relation between $\omega\,\Delta\,t$ and $\tilde{\omega}\,\Delta\,t$ is not one to one.

needed. If we select β_0 as a free parameter, according to eq. (32), $\frac{\partial E_1}{\partial \beta_0}$ should be equal to zero. Eq. (26) should be satisfied for $r = 0$, 1 and 2. Thus, first it is necessary to calculate the relation between β_1, β_2 and β_3 on one hand, and β_0 on the other hand using eq. (26). Then, using equation $\frac{\partial E_1}{\partial \beta_0} = 0$, it is possible to determine all coefficients:

$$\beta_0 = 2.30256, \quad \beta_1 = -3\beta_0 + \frac{53}{12} = -2.49100,$$

$$\beta_2 = 3\beta_0 - \frac{16}{3} = 1.57434, \quad \beta_3 = -\beta_0 + \frac{23}{12} = -0.38589. \tag{33}$$

In this calculation $\chi = 0.36$. Fig. 4 shows the relation between $\tilde{\omega}$ and ω for the calculated coefficients. For a given $\tilde{\omega}\,\Delta t$, there are four values of $\omega\,\Delta t$ which satisfy relation (30). One of the roots has positive imaginary part for $\tilde{\omega}\,\Delta t > 0.4$. Tam & Webb (1993) showed that this root can cause numerical instability. They pointed out that instability can be prevented by imposing a sufficient condition

$$\mathrm{Im}\,(\omega_k\,\Delta t) \leq 0 \quad k = 1, 2, 3, 4 \tag{34}$$

4.1.3 Partial summary on the first approach

Independently of method of calculating unknown coefficients (TE or DRP), the first approach to approximating temporal derivative leads to spurious numerical solution that can cause instability. An application of the DRP criterion leads to the system of nonlinear eq. (32) for unknown coefficients. The nonlinearity restricts us to calculate only one of the coefficients according to the DRP criterion. In other words, the application of the DRP criterion in the first approach cannot be effective.

4.2 The second approach

By using eq. (23) instead of (21), we can avoid the spurious numerical solution and the difficulty of solving system of nonlinear eq. (32).

4.2.1 Approximation of temporal derivatives using Taylor expansion

Application of the TE to eq. (23) leads to the following system of equations for determining coefficients b_j:

$$\sum_{j=N}^{1} j^r\, b_j = \delta_{1r}\ , r = 0, \ldots, 1 - N. \tag{35}$$

Approximation (23) is accurate up to order $(\Delta t)^{\text{order}}$ where order $= 1 - N$.

4.2.2 Approximation of temporal derivatives using DRP criterion

Applying the temporal Fourier transform

$$\tilde{f}(\omega) = \frac{1}{2\pi} \int_{-\infty}^{+\infty} f(t)\, e^{-\mathrm{i}\omega t} \mathrm{d}t \tag{36}$$

to eq. (23) we obtain

$$\mathrm{i}\omega \tilde{f} \approx \left(\frac{1}{\Delta t} \sum_{j=N}^{M=1} b_j\, e^{\mathrm{i}\, j\omega\, \Delta t} \right) \tilde{f}. \tag{37}$$

The expression in the parentheses can be considered $\mathrm{i}\tilde{\omega}$, where $\tilde{\omega}$ may be defined as a numerical frequency:

$$\tilde{\omega} = \frac{-\mathrm{i}}{\Delta t} \sum_{j=N}^{M=1} b_j e^{\mathrm{i}\, j\, \omega\, \Delta t}. \tag{38}$$

$\tilde{\omega}\, \Delta t$ is a periodic function of $\omega\, \Delta t$ with period 2π. Let us point out that the relation between $\tilde{\omega}$ and ω in eq. (38) is one to one—unlike relation (30). This is a very important benefit of using eq. (23) instead of eq. (21).

In order to have the numerical and true frequencies as close as possible in a range $[A, B]$, we can define error

$$E_1 \equiv \int_A^B \left\{ \chi (\mathrm{Re}\, [\omega\, \Delta t - \tilde{\omega}\, \Delta t])^2 + (1 - \chi)\, (\mathrm{Im}\, [\omega\, \Delta t - \tilde{\omega}\, \Delta t])^2 \right\} \mathrm{d}\, (\omega\, \Delta t)\,. \tag{39}$$

A and B are dimensionless numbers. Similarly as in the case of error (10) for the spatial approximation, we consider also here a general range $[A, B]$ whereas Tam & Webb (1993) used $[-0.5,0.5]$.

We can find unknown coefficients b_j by minimizing error (39). Condition

$$\frac{\partial E_1}{\partial b_j} = 0, \;\; j = N, \ldots, 1 \tag{40}$$

provides a system of linear algebraic equations for coefficients b_j.

We can rewrite eq. (39):

$$E_1 = \int_A^B \left\{ \chi \left(\mathrm{Re} \left[\zeta + \mathrm{i} \sum_{j=N}^{M=1} b_j e^{\mathrm{i}\, j\, \zeta} \right] \right)^2 + (1 - \chi) \left(\mathrm{Im} \left[\zeta + \mathrm{i} \sum_{j=N}^{M=1} b_j e^{\mathrm{i}\, j\, \zeta} \right] \right)^2 \right\} \mathrm{d}\zeta$$

$$= \int_A^B \left\{ \chi \left(\zeta - \sum_{j=N}^{M=1} b_j \sin(j\zeta) \right)^2 + (1 - \chi) \left(\sum_{j=N}^{M=1} b_j \cos(j\zeta) \right)^2 \right\} \mathrm{d}\zeta. \tag{41}$$

Using eq. (41) it is possible to simplify eq. (40):

$$\frac{\partial E_1}{\partial b_s} = \int_A^B \left\{ -2\chi \left(\zeta - \sum_{j=N}^{M=1} b_j \sin(j\zeta) \right) \sin(s\zeta) + 2\,(1 - \chi) \left(\sum_{j=N}^{M=1} b_j \cos(j\zeta) \right) \cos(s\zeta) \right\} \mathrm{d}\zeta = 0. \tag{42}$$

This can be further rearranged as

$$\int_A^B \chi\zeta \sin(s\zeta)\, d\zeta = \sum_{j=N}^{M=1} b_j \left\{ \int_A^B [\chi \sin(j\zeta) \sin(s\zeta) + (1 - \chi) \cos(j\zeta) \cos(s\zeta)] \mathrm{d}\zeta \right\}. \tag{43}$$

If we define

$$G_{sj} \equiv \int_A^B [\chi \sin(j\zeta) \sin(s\zeta) + (1 - \chi) \cos(j\zeta) \cos(s\zeta)] \mathrm{d}\zeta$$

and

$$d_s \equiv \int_A^B \chi\zeta \sin(s\zeta)\, \mathrm{d}\zeta,$$

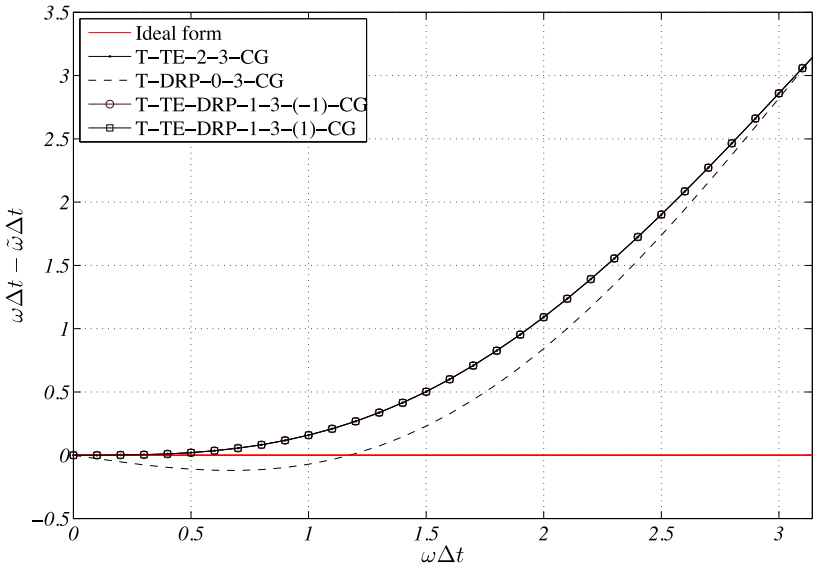

Figure 5. The real part of difference $\omega\,\Delta t - \tilde{\omega}\,\Delta t$ as a function of $\omega\,\Delta\,t$ for four collocated-grid approximations: T-TE-2-3-CG—TE second-order 3-point ($N = -1,\ M = 1$), T-DRP-0-3-CG—DRP 0th-order 3-point ($N = -1,\ M = 1$), T-DRP-1-3-(-1)-CG—combined TE-DRP first-order 3-point ($N = -1,\ M = 1$) with coefficient b_{-1} calculated as a free parameter and T-DRP-1-3-(1)-CG—combined TE and DRP first-order 3-point ($N = -1,\ M = 1$) with coefficient b_1 calculated as a free parameter. In the DRP approximations, range $[A, B]$ and χ are $[-\pi/2, \pi/2]$ and 0.5, respectively.

Eq. (43) takes a simple form of a system of linear algebraic equations for coefficients b_j:

$$\sum_{j=N}^{M=1} G_{sj} b_j = d_s \quad s = N, \ldots, 1$$

$$\begin{cases} G_{sj} = (s\chi - j\chi - s)\dfrac{\cos(A\,j)\,\sin(A\,s) - \cos(B\,j)\,\sin(B\,s)}{s^2 - j^2} \\ \qquad + (s\chi - j\chi + j)\dfrac{\cos(As)\,\sin(A\,j) - \cos(B\,s)\,\sin(B\,j)}{s^2 - j^2} & j \neq \pm s \\ G_{sj} = \dfrac{B - A}{2} + (2\chi - 1)\,\dfrac{\sin(2\,A\,s) - \sin(2\,B\,s)}{4s} & j = s \neq 0 \\ G_{sj} = (2\chi - 1)\,\dfrac{A - B}{2} + \dfrac{-\sin(2\,A\,s) + \sin(2\,B\,s)}{4s} & j = -s \neq 0 \\ G_{sj} = (A - B)(\chi - 1) & j = s = 0 \end{cases} \tag{44}$$

$$\begin{cases} d_s = 0 & s = 0 \\ d_s = \chi\,\dfrac{A\,\cos(A\,s) - B\,\cos(B\,s)}{s} - \chi\,\dfrac{\sin(A\,s) - \sin(B\,s)}{s^2} & s \neq 0 \end{cases}$$

4.2.3 Combination of the DRP criterion and Taylor expansion

By minimizing error (39), we do not ensure consistency of approximation that is quantified by the order of approximation in the TE approach. For ensuring such consistency, it is possible to combine the TE approach with the DRP criterion. We can choose *NFP* coefficients, say free parameters, to satisfy eq. (40), and consequently eq. (44), in order to minimize error (39). Hence, eq. (35) should be satisfied for $r = 0, \ldots, 1 - N - NFP$. The all coefficients are thus determined by solving one system of equations that is a combination of eq. (44) for $s =$ subscripts of free parameters and eq. (35) for $r = 0, \ldots, 1 - N - NFP$. Due to the choice of *NFP* free parameters the order of accuracy decreases to $1 - N - NFP$.

Consider an example. It is obvious from approximation (23) that always $M = 1$. Let us choose, for example, $N = -3$. If we want that the approximation (23) be $(\Delta t)^2$ accurate, this leaves two coefficients as free parameters. It means that eq. (35) should be satisfied for $r = 0, 1, 2$. It is possible to choose two free parameters in a way that minimizes error E_1, eq. (39). We can select any two of the four coefficients as free parameters. Taking, for example, b_0 and b_{-2} as free parameters, $\partial E_1/\partial b_0$ and $\partial E_1/\partial b_{-2}$ should be equal to zero. It means that eq. (44) should be satisfied for $s = 0,\ -2$.

Let us point out that it is not usual to consider more than 3 points for approximation of the temporal derivative on CG in seismic wave modelling.

Note that the explanation on the order of approximation in the symmetric case in Section 3.3 is also true here for the case of symmetry in coefficients and free parameters including b_0; in the case of symmetry considering b_0 as a free parameter has no practical meaning.

Fig. 5 illustrates the real part of difference $\omega\,\Delta t - \tilde{\omega}\,\Delta t$ as a function of $\omega\,\Delta t$ for four alternative 3-point approximations on the CG: T-TE-2-3-CG—TE second-order 3-point ($N = -1,\ M = 1$), T-DRP-0-3-CG—DRP 0th-order 3-point ($N = -1,\ M = 1$), T-TE-DRP-1-3-(-1)-CG—combined TE-DRP first-order 3-point ($N = -1,\ M = 1$) with coefficient b_{-1} calculated as a free parameter, and T-TE-DRP-1-3-(1)-CG—combined TE-DRP first-order 3-point ($N = -1,\ M = 1$) with coefficient b_1 calculated as a free parameter. In the DRP approximations, range $[A,\ B]$ and χ are $[-\pi/2,\ \pi/2]$ and 0.5, respectively. Note that capital T indicates the temporal derivative.

For T-DRP-0-3-CG, in comparison with the three other approximations, the range of $\omega\,\Delta t$ with acceptably small values of $\omega\,\Delta t - \tilde{\omega}\,\Delta t$ is larger. The three other approximations have the same difference, although their coefficients are different.

4.2.4 Partial summary on the second approach

In the second approach to approximating temporal derivative, the application of the DRP criterion does not have problem of the first approach. The second approach makes it possible to consider more than one coefficient as a free parameter. Moreover, we can obtain one system of linear equations for calculating coefficients by requiring the numerical frequency being as close as possible to the true frequency. For having consistency in the TE-approach sense, we can combine this system of linear equations with condition (35). However, the application of the DRP criterion cannot give better than the first-order accuracy (that matches T-TE-2-3-CG in terms of the $\omega\,\Delta t - \tilde{\omega}\,\Delta t$ difference) if we use not more than 3 time levels ($M = 1$, $N = -1$, the updated time level is calculated from two previous time levels).

5 APPROXIMATION OF DERIVATIVES BASED ON TAYLOR EXPANSION AND DRP CRITERION ON THE STAGGERED GRID

5.1 Approximation of spatial derivatives

For approximating the first spatial derivative of a field variable f at grid position $x = I\,\Delta x$, we can use values of this variable at neighbouring grid points at $x \pm j\,\Delta x$; $j = 1/2,\ 3/2,\ 5/2, \ldots$. An approximation of the first spatial derivative may be written as

$$\left(\frac{\partial f}{\partial x}\right)_I \approx \frac{1}{\Delta x}\sum_{j=N}^{M} a_j\, f_{I+j} \tag{45}$$

or, equivalently,

$$\frac{\partial f}{\partial x}(x) \approx \frac{1}{\Delta x}\sum_{j=N}^{M} a_j\, f(x + j\Delta x)\,, \tag{46}$$

where $N = -(2n+1)/2$ and $M = (2n+1)/2$, with $n \in \{0, 1, 2, 3, \ldots\}$. The two latter equations are similar to eqs (3) and (4), the only difference being in the nature of N and M: they are integers in eqs (3) and (4). Consequently, an application of the TE leads to eq. (6) for finding coefficients. Similarly, an application of the DRP criterion leads to eq. (16). The only difference is that situation with $s = 0$ in eq. (17) cannot occur in the case of the SG. Similarly to Section 3.3 we can combine the TE approach with the DRP criterion.

Let us make note on the order of approximation on the SG. Consider the TE approach. If $N \neq -M$, eq. (6) should be satisfied for $r = 0, \ldots, M - N$ and the order of accuracy is $M - N$. If $N = -M$, eq. (6) should be satisfied for $r = 0, \ldots, M - N$ as well but the order of accuracy is $M - N + 1$. This is because in this case eq. (6) is automatically satisfied for $r = M - N + 1$.

Consider now the TE-DRP combination. If coefficients are asymmetric, that is, if $N \neq -M$ or $N = -M$ but the free parameters are not symmetric, eq. (6) should be satisfied for $r = 0, \ldots, M - N - NFP$ and the order of accuracy is $M - N - NFP$. If coefficients are symmetric, that is, $N = -M$ and free parameters are symmetric, eq. (6) should be satisfied for $r = 0, \ldots, M - N - NFP$ but the order of accuracy is $M - N + 1 - NFP$.

Fig. 6 shows the real part of difference $k\,\Delta x - \tilde{k}\,\Delta x$ as a function of $k\Delta x$ for four staggered-grid approximations: S-TE-2-2-SG—TE second-order 2-point ($N = -0.5,\ M = 0.5$), S-TE-4-4-SG—TE fourth-order 4-point ($N = -1.5,\ M = 1.5$), S-DRP-0-4-SG—DRP 0th-order 4-point ($N = -1.5,\ M = 1.5$) and S-TE-DRP-2-4-(-0.5,0.5)-SG—combined TE-DRP second-order 4-point ($N = -1.5,\ M = 1.5$) with coefficients $a_{-0.5}$ and $a_{0.5}$ calculated as free parameters.

The range of $k\Delta x$ with 'acceptably small' values of $k\Delta x - \tilde{k}\,\Delta x$ increases from S-TE-2-2-SG through S-TE-4-4-SG and S-TE-DRP-2-4-(−0.5,0.5)-SG and is the largest for S-DRP-0-4-SG.

We can see that the use of the L_1 error norm in the TE approach and L_2 error norm in the DRP approach lead to similar results as we saw for the collocated-grid approximations. For a fixed number of points, the use of the DRP criterion, as compared to the TE approximation, increases the acceptable range of $k\Delta x$ but decreases the order of approximation.

Now we can compare the approximations on the SG and CG. Fig. 7 compares the real part of difference $k\,\Delta x - \tilde{k}\,\Delta x$ as a function of $k\,\Delta x$ for six approximations: S-TE-4-5-CG, S-DRP-0-5-CG, S-TE-DRP-2-5-(−1,1)-CG, S-TE-4-4-SG, S-DRP-0-4-SG, and S-TE-DRP-2-4-(−0.5,0.5)-SG. The use of the SG approximations, as compared to the CG approximations, increases ranges of $k\Delta x$ with acceptably small values of $k\Delta x - \tilde{k}\,\Delta x$ while does not decrease the order of approximation.

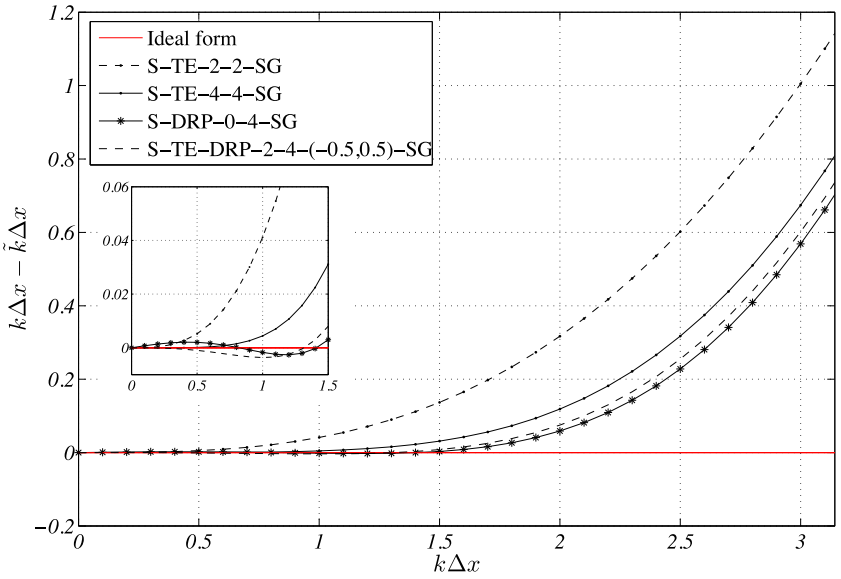

Figure 6. The real part of difference $k\,\Delta x - \tilde{k}\,\Delta x$ as a function of $k\,\Delta x$ for four staggered-grid approximations: S-TE-2-2-SG—TE second-order 2-point ($N = -0.5,\ M = 0.5$), S-TE-4-4-SG—TE fourth-order 4-point ($N = -1.5,\ M = 1.5$), S-DRP-0-4-SG—DRP 0th-order 4-point ($N = -1.5,\ M = 1.5$) and S-TE-DRP-2-4-(-0.5,0.5)-SG—combined TE-DRP second-order 4-point ($N = -1.5,\ M = 1.5$) with coefficients $a_{-0.5}$ and $a_{0.5}$ calculated as free parameters. In the DRP approximations, $[A,\ B] = [-\pi/2, \pi/2]$.

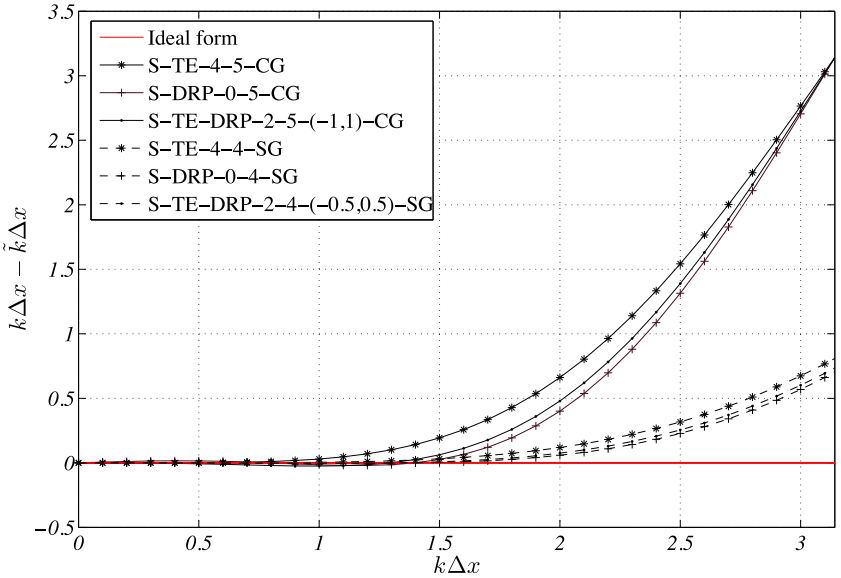

Figure 7. The real part of difference $k\,\Delta x - \tilde{k}\,\Delta x$ as a function of $k\,\Delta x$ for six approximations—illustrative comparison of the TE and DRP-criterion approximations on the staggered and collocated grids: S-TE-4-5-CG, S-DRP-0-5-CG, S-TE-DRP-2-5-(-1,1)-CG, S-TE-4-4-SG, S-DRP-0-4-SG and S-TE-DRP-2-4-(-0.5,0.5)-SG.

5.2 Approximation of temporal derivatives

In the SG, some variables are shifted in time with respect to the others by $\Delta t/2$**.** Here, for approximating the first temporal derivative of a field variable f at time $t = m\,\Delta t$, we use values of the variable at previous times $t - j\,\Delta t;\ j = 1/2,\ 3/2,\ 5/2, \ldots$ and at time $t + \Delta t/2$. The approximation of the first temporal derivative may be written as

$$\left(\frac{\partial f}{\partial t}\right)^m \approx \frac{1}{\Delta t} \sum_{j=N}^{M=\frac{1}{2}} b_j\, f^{m+j} \tag{47}$$

or, equivalently,

$$\frac{\partial f}{\partial t}(t) \approx \frac{1}{\Delta t} \sum_{j=N}^{M=\frac{1}{2}} b_j\, f(t + j\Delta t)\,, \tag{48}$$

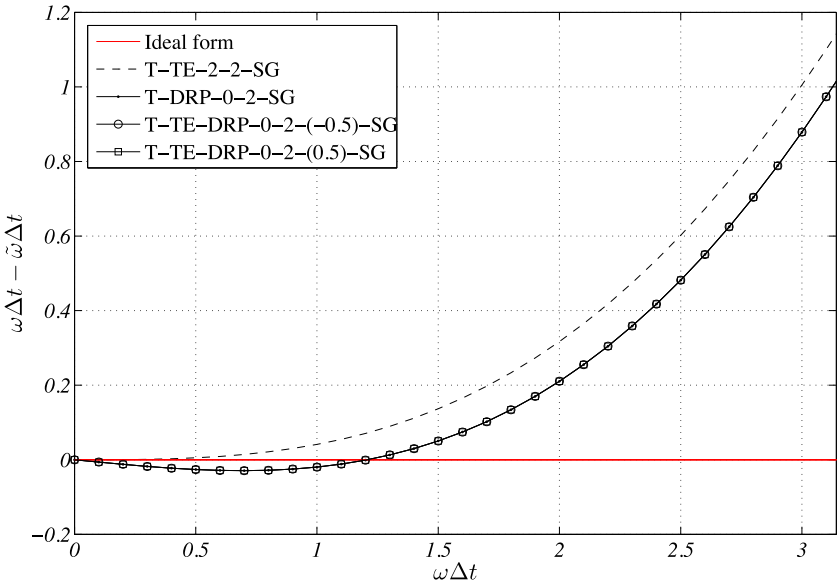

Figure 8. The real part of difference $\omega\,\Delta t - \tilde{\omega}\,\Delta t$ as a function of $\omega\,\Delta t$ for four staggered-grid approximations: T-TE-2-2-SG—TE second-order 2-point ($N = -0.5,\ M = 0.5$), T-DRP-0-2-SG—DRP 0th-order 2-point ($N = -0.5,\ M = 0.5$), T-TE-DRP-0-2-(-0.5)-SG—combined TE-DRP 0th-order 2-point ($N = -0.5,\ M = 0.5$) with coefficient $b_{-0.5}$ calculated as a free parameter, T-TE-DRP-0-2-(0.5)-SG—combined TE-DRP 0th-order 2-point ($N = -0.5,\ M = 0.5$) with coefficient $b_{0.5}$ calculated as a free parameter. In the DRP approximations, range $[A, B]$ and χ are $[-\pi/2, \pi/2]$ and 0.5, respectively.

where $N = -(2n + 1)/2$ and $n \in \{0, 1, 2, 3, \ldots\}$. The two latter approximating equations are similar to approximations (22) and (23), the only difference being in the nature of N and M:N is an integer and $M = 1$ in eqs (22) and (23). Because eqs (23) and (48) have the same form, we can use eqs (35) and (44) for calculating unknown coefficients b_j in eq. (48) based on TE and DRP criterion, respectively. It is possible to combine eqs (35) and (44), that is, the TE and DRP approaches, for having consistency.

Note that cases $s = 0$ and $j = s = 0$, see eqs (44), cannot occur in the SG. Note also that the explanation in Section 5.1 on the order of approximation on the SG is also true here.

Fig. 8 illustrates the real part of difference $\omega\,\Delta t - \tilde{\omega}\,\Delta t$as a function of $\omega\,\Delta t$ for four alternative 2-point staggered-grid approximations of temporal derivative: T-TE-2-2-SG—TE second-order 2-point ($N = -0.5,\ M = 0.5$), T-DRP-0-2-SG—DRP 0th-order 2-point ($N = -0.5,\ M = 0.5$), T-TE-DRP-0-2-(-0.5)-SG—combined TE-DRP 0th-order 2-point ($N = -0.5,\ M = 0.5$) with coefficient $b_{-0.5}$ calculated as a free parameter, and T-TE-DRP-0-2-(0.5)-SG—combined TE-DRP 0th-order 2-point ($N = -0.5,\ M = 0.5$) with coefficient $b_{0.5}$ calculated as a free parameter. For T-TE-2-2-SG, in comparison with the three other approximations, the range of $\omega\Delta t$ with acceptably small values of $\omega\,\Delta t - \tilde{\omega}\,\Delta t$ is narrower. The three other approximations have the same difference and coefficients.

Now we can compare the approximations on the SG and CG. Fig. 9 illustrates the real part of difference $\omega\,\Delta t - \tilde{\omega}\,\Delta t$ as a function of $\omega\,\Delta t$ for four approximations of the temporal derivative. We can see that the staggered-grid approximations behave better than the collocated-grid approximations.

5.3 Partial summary

In Section 5, we derived formulae for approximating spatial and temporal derivatives on the SG and equations for determining coefficients based on TE, DRP and TE-DRP approaches. We obtained the same equations as those for the CG. We analysed the TE and DRP approximations on the SG. We compared the approximations on the CG and SG. We may point out that the use of the staggered-grid approximations, as compared to the collocated-grid approximations, increases ranges of $k\Delta x$ and $\omega\,\Delta t$ with acceptably small values of $k\Delta x - \tilde{k}\,\Delta x$ and $\omega\,\Delta t - \tilde{\omega}\,\Delta t$, respectively, while does not decrease the order of approximation.

6 FINITE-DIFFERENCE SCHEMES

Based on the developed approximations we can now construct FD schemes. For numerical comparison, we include all the basic schemes that use 2 or 4 spatial grid points in SG, and 3 or 5 or 7 points in CG. It is reasonable to use two time levels in SG and three time levels in CG. Fig. 10 shows structure of all schemes for which we have performed numerical tests.

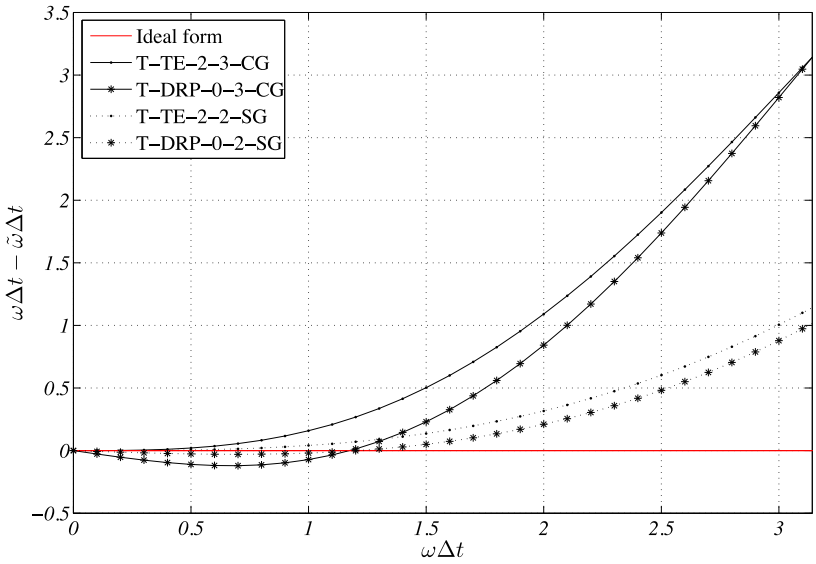

Figure 9. The real part of difference $\omega\Delta t - \tilde{\omega}\Delta t$ as a function of $\omega\,\Delta t$ for four approximations of temporal derivatives—illustrative comparison of the TE and DRP-criterion approximations on the staggered and collocated grids: T-TE-2-3-CG, T-DRP-0-3-CG, T-TE-2-2-SG and T-DRP-0-2-SG. In the DRP approximations, range $[A, B]$ and χ are $[-\pi/2, \pi/2]$ and 0.5, respectively.

FD schemes								
TE		DRP		TE-DRP				
order		order		order		# of points		grid type
in time	in space	in time	in space	in time	in space	in time	in space	
2	2	0	0	N. A.		2	2	staggered
2	4	0	0	0	2	2	4	
				2	2			
2	2	0	0	N. A.		3	3	collocated
2	4	0	0	2	2	3	5	
2	4	0	0	2	2	3	7	

Figure 10. Types, orders of accuracy, the numbers of points and types of grids of the analysed FD schemes. To illustrate the structure of the set of the considered schemes, the shadowed cells indicate the FD scheme TE-DRP-2-2-2-4-SG.

6.1 FD schemes on the collocated grid

Let Δx and Δt be the grid spacing and time step. Let V_I^m, T_I^m and F_I^m be discrete approximations of the particle velocity, stress and body force at position $x = I\Delta x$ and time $t = m\Delta t$ in the CG. Let N_{Space}, M_{Space} and N_{Time} be integers. Using approximations (3) and (22) for the spatial and temporal derivatives, respectively, eq. (2) may be approximated on the CG by

$$\left(\frac{\rho_I}{\Delta t}\sum_{j=N_{\text{Time}}}^{1} b_j\, V_I^{m+j}\right) = \left(\frac{1}{\Delta x}\sum_{j=N_{\text{Space}}}^{M_{\text{Space}}} a_j\, T_{I+j}^m\right) + F_I^m,$$

$$\left(\frac{1}{\Delta t}\sum_{j=N_{\text{Time}}}^{0} b_j\, T_I^{m+j}\right) = C_I\left(\frac{1}{\Delta x}\sum_{j=N_{\text{Space}}}^{M_{\text{Space}}} a_j\, V_{I+j}^m\right). \tag{49}$$

A rearrangement gives

$$V_I^{m+1} = \frac{\Delta t}{b_1\,\Delta x\,\rho_I}\left(\sum_{j=N_{\text{Space}}}^{M_{\text{Space}}} a_j\, T_{I+j}^m\right) - \frac{1}{b_1}\left(\sum_{j=N_{\text{Time}}}^{0} b_j\, V_I^{m+j}\right) + \frac{\Delta t}{b_1\,\rho_I}F_I^m,$$

$$T_I^{m+1} = \frac{C_I\,\Delta t}{b_1\,\Delta x}\left(\sum_{j=N_{\text{Space}}}^{M_{\text{Space}}} a_j\, V_{I+j}^m\right) - \frac{1}{b_1}\left(\sum_{j=N_{\text{Time}}}^{0} b_j\, T_I^{m+j}\right). \tag{50}$$

Coefficients a_j can be determined using either of three approaches—TE, eq. (6), DRP, eq. (16) and the TE-DRP combination. Similarly, coefficients b_j can be calculated using either of three approaches—TE, eq. (35), DRP, eq. (44) and the TE-DRP combination.

We numerically test the following collocated-grid schemes:

(1) TE-2-2-3-3-CG

TE second-order in time, TE second-order in space, 3-point in time ($M_{\text{Time}} = -N_{\text{Time}} = 1$), 3-point in space ($M_{\text{Space}} = -N_{\text{Space}} = 1$)

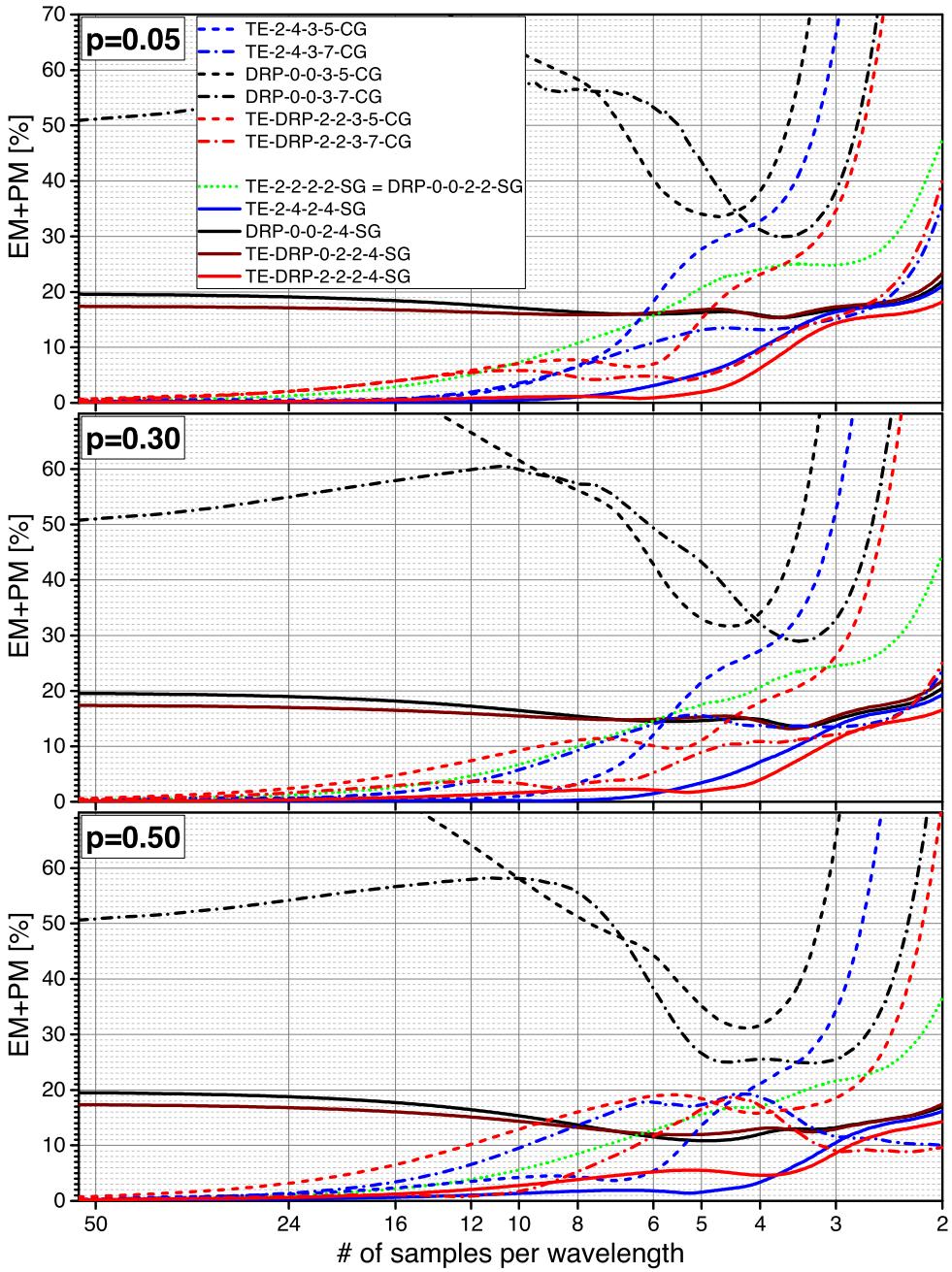

Figure 11. The sum of the envelope misfit (EM) and phase misfit (PM), in the range of [0,70] per cent, as a function of the number of grid spacings per wavelength for three values of the stability ratio: $p \in \{0.05,\ 0.3,\ 0.5\}$.

(2) TE-2-4-3-5-CG

TE second-order in time, TE fourth-order in space, 3-point in time ($M_{\text{Time}} = -N_{\text{Time}} = 1$), 5-point in space ($M_{\text{Space}} = -N_{\text{Space}} = 2$)

(3) TE-2-4-3-7-CG

TE second-order in time, TE fourth-order in space, 3-point in time ($M_{\text{Time}} = -N_{\text{Time}} = 1$), 7-point in space – averaging of ($N_{\text{Space}} = -3$, $M_{\text{Space}} = 1$) and ($N_{\text{Space}} = -1$, $M_{\text{Space}} = 3$)

(4) DRP-0-0-3-3-CG

DRP 0th-order in time, DRP 0th-order in space, 3-point in time ($M_{\text{Time}} = -N_{\text{Time}} = 1$), 3-point in space ($M_{\text{Space}} = -N_{\text{Space}} = 1$)

(5) DRP-0-0-3-5-CG

DRP 0th-order in time, DRP 0th-order in space, 3-point in time ($M_{\text{Time}} = -N_{\text{Time}} = 1$), 5-point in space ($M_{\text{Space}} = -N_{\text{Space}} = 2$)

(6) DRP-0-0-3-7-CG

DRP 0th-order in time, DRP 0th-order in space, 3-point in time ($M_{\text{Time}} = -N_{\text{Time}} = 1$), 7-point in space — averaging of ($N_{\text{Space}} = -3$, $M_{\text{Space}} = 1$) and ($N_{\text{Space}} = -1$, $M_{\text{Space}} = 3$)

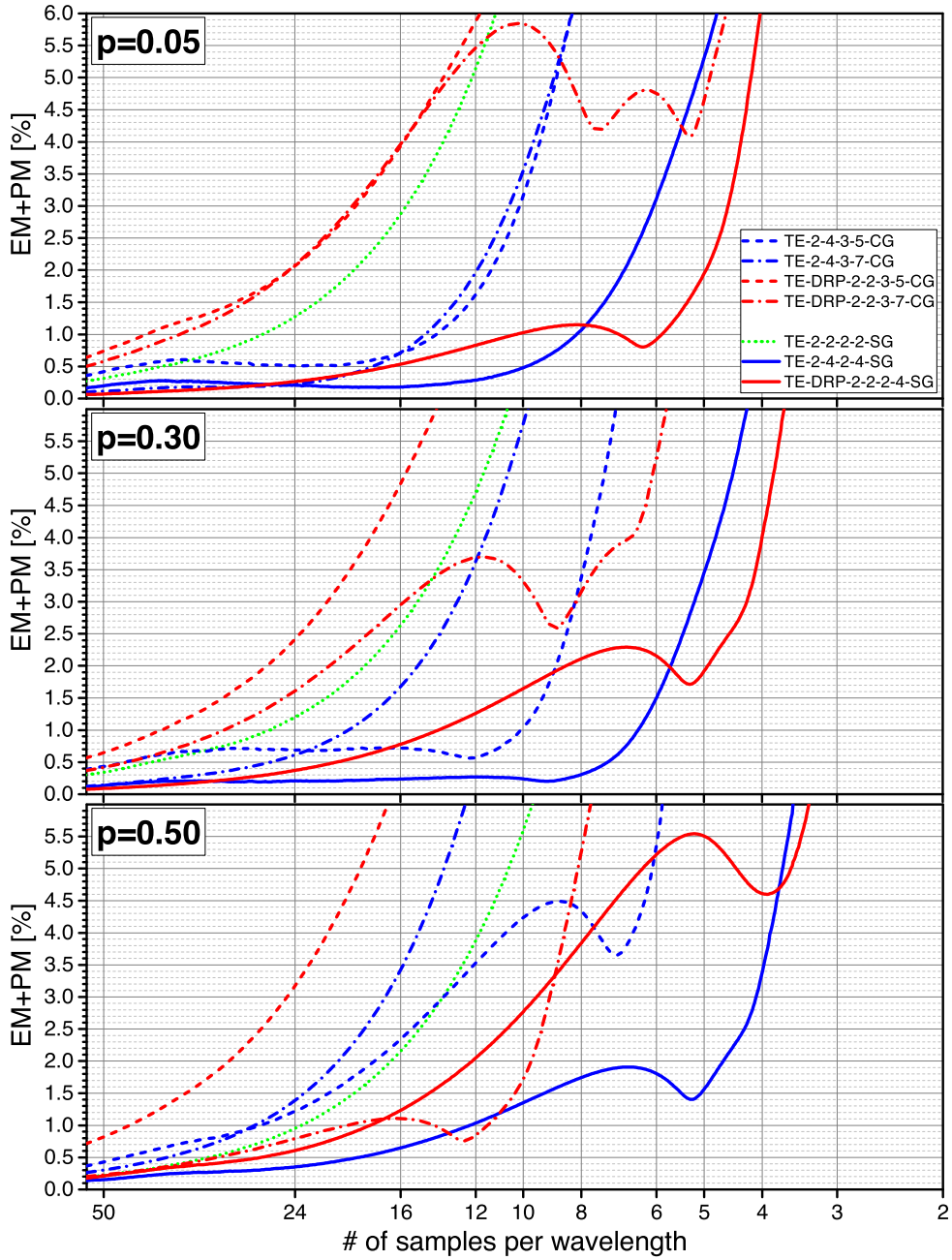

Figure 12. The sum of the envelope misfit (EM) and phase misfit (PM), in the range of [0,6] per cent, as a function of the number of grid spacings per wavelength for three values of the stability ratio: $p \in \{0.05,\ 0.3,\ 0.5\}$.

(7) TE-DRP-2-2-3-5-CG

TE second-order in time, combined TE-DRP second-order in space, 3-point in time ($M_{\text{Time}} = -N_{\text{Time}} = 1$), 5-point in space ($M_{\text{Space}} = -N_{\text{Space}} = 2$) with a_{-1} and a_1 being free parameters

(8) TE-DRP-2-2-3-7-CG

TE second-order in time, combined TE-DRP second-order in space, 3-point in time($M_{\text{Time}} = -N_{\text{Time}} = 1$), 7-point in space – averaging of ($N_{\text{Space}} = -3$, $M_{\text{Space}} = 1$) and ($N_{\text{Space}} = -1$, $M_{\text{Space}} = 3$) with a_{-1} and a_1 being free parameters

The schemes are given in Appendix C.

6.2 FD schemes on the staggered grid

Eq. (2) may be approximated on the SG using approximations (45) and (47). Assume now N_{Space}, M_{Space} and N_{Time} in the form $(2n + 1)/2$ with n being an integer. Instead of eq. (50), we obtain

Dispersion relations and stability conditions					
dim.	scheme	dispersion relation	time step	max. value of Courant number	stability ratio
		$S_\omega^2 =$	$\Delta t =$	$S_M =$	p
1D	TE-2-4-2-4-SG	$\left(\frac{\Delta t}{h}c\right)^2 S_4^2$	$p\frac{h}{c}S_M$	$\frac{6}{7}$	$0 < p \le 1$
	TE-DRP-2-2-2-4-SG	$\left(\frac{\Delta t}{h}c\right)^2 S_o^2$		$\frac{6}{7.2192}$	
3D	TE-2-4-2-4-SG	$\left(\frac{\Delta t}{h}\beta\right)^2\left(S_x^2+S_y^2+S_z^2\right)$ $\left(\frac{\Delta t}{h}\alpha\right)^2\left(S_x^2+S_y^2+S_z^2\right)$	$p\frac{h}{\alpha}S_M$	$\frac{6}{7\sqrt{3}}$	
	TE-DRP-2-2-2-4-SG	$\left(\frac{\Delta t}{h}\beta\right)^2\left(S_{ox}^2+S_{oy}^2+S_{oz}^2\right)$ $\left(\frac{\Delta t}{h}\alpha\right)^2\left(S_{ox}^2+S_{oy}^2+S_{oz}^2\right)$		$\frac{6}{7.2192\sqrt{3}}$	
$S_\omega = \sin\left(\frac{1}{2}\tilde{\omega}\,\Delta\right)$ $S_4 = \frac{9}{8}\sin\left(\frac{1}{2}kh\right) - \frac{1}{24}\sin\left(\frac{3}{2}kh\right)$ $S_o = 1.1524\sin\left(\frac{1}{2}kh\right) - 0.0508\sin\left(\frac{3}{2}kh\right)$ $S_\xi = \frac{9}{8}\sin\left(\frac{1}{2}k_\xi h\right) - \frac{1}{24}\sin\left(\frac{3}{2}k_\xi h\right)$ $S_{o\xi} = 1.1524\sin\left(\frac{1}{2}k_\xi h\right) - 0.0508\sin\left(\frac{3}{2}k_\xi h\right)$ $\xi \in \{x, y, z\}$					

Figure 13. Dispersion relations and stability conditions for the two FD schemes in 1-D and 3-D. Here, α and β are the *P*- and *S*-wave speeds, $\tilde{\omega}$ is grid angular frequency, k is true wavenumber and k_x, k_y, k_z are components of the wavenumber vector.

$$V_I^{m+\frac{1}{2}} = \frac{\Delta t}{b_{\frac{1}{2}}\,\Delta x\,\rho_I}\left(\sum_{j=N_{\text{Space}}}^{M_{\text{Space}}} a_j\, T_{I+j}^m\right) - \frac{1}{b_{\frac{1}{2}}}\left(\sum_{j=N_{\text{Time}}}^{-\frac{1}{2}} b_j\, V_I^{m+j}\right) + \frac{\Delta t}{b_{\frac{1}{2}}\,\rho_I}F_I^m,$$

$$T_{I-\frac{1}{2}}^m = \frac{C_{I-\frac{1}{2}}\,\Delta t}{b_{\frac{1}{2}}\,\Delta x}\left(\sum_{j=N_{\text{Space}}}^{M_{\text{Space}}} a_j\, V_{I-\frac{1}{2}+j}^{m-\frac{1}{2}}\right) - \frac{1}{b_{\frac{1}{2}}}\left(\sum_{j=N_{\text{Time}}}^{-\frac{1}{2}} b_j\, T_{I-\frac{1}{2}}^{m-\frac{1}{2}+j}\right). \tag{51}$$

Analogously, coefficients a_j can be determined using either of three approaches—TE, eq. (6), DRP, eq. (16) and the TE-DRP combination. Similarly, coefficients b_j can be calculated using either of three approaches—TE, eq. (35), DRP, eq. (44) and the TE-DRP combination.

We numerically test the following staggered-grid schemes:

(1) TE-2-2-2-2-SG
TE second-order in time, TE second-order in space, 2-point in time ($M_{\text{Time}} = -N_{\text{Time}} = 1/2$), 2-point in space ($M_{\text{Space}} = -N_{\text{Space}} = 1/2$)
(2) TE-2-4-2-4-SG
TE second-order in time, TE fourth-order in space, 2-point in time ($M_{\text{Time}} = -N_{\text{Time}} = 1/2$), 4-point in space ($M_{\text{Space}} = -N_{\text{Space}} = 3/2$)
(3) DRP-0-0-2-2-SG
DRP 0th-order in time, DRP 0th-order in space, 2-point in time ($M_{\text{Time}} = -N_{\text{Time}} = 1/2$), 2-point in space ($M_{\text{Space}} = -N_{\text{Space}} = 1/2$)
(4) DRP-0-0-2-4-SG
DRP 0th-order in time, DRP 0th-order in space, 2-point in time ($M_{\text{Time}} = -N_{\text{Time}} = 1/2$), 4-point in space ($M_{\text{Space}} = -N_{\text{Space}} = 3/2$)
(5) TE-DRP-0-2-2-4-SG
combined TE and DRP 0th-order in time, combined TE-DRP second-order in space, 2-point in time ($M_{\text{Time}} = -N_{\text{Time}} = 1/2$) with $b_{-1/2}$ being free parameter, 4-point in space ($M_{\text{Space}} = -N_{\text{Space}} = 3/2$) with $a_{-1/2}$ and $a_{1/2}$ being free parameters
(6) TE-DRP-2-2-2-4-SG
TE second-order in time, combined TE-DRP second-order in space, 2-point in time ($M_{\text{Time}} = -N_{\text{Time}} = 1/2$), 4-point in space ($M_{\text{Space}} = -N_{\text{Space}} = 3/2$) with $a_{-1/2}$ and $a_{1/2}$ being free parameters

The schemes are given in Appendix C.

Normalized grid phase velocity		
dim.	scheme	normalized grid phase velocity
1D	TE-2-4-2-4-SG	$\frac{\tilde{c}}{c} = \frac{7}{6}\frac{N_\lambda}{\pi p}\arcsin\left(p\frac{6}{7}S_4\right)$
	TE-DRP-2-2-2-4-SG	$\frac{\tilde{c}}{c} = \frac{7.2192}{6}\frac{N_\lambda}{\pi p}\arcsin\left(p\frac{6}{7.2192}S_o\right)$
3D	TE-2-4-2-4-SG	$\frac{\tilde{\alpha}}{\alpha} = \frac{7\sqrt{3}}{6}\frac{r N_\lambda^S}{\pi p}\arcsin\left[p\frac{6}{7\sqrt{3}}\sqrt{S_x^2+S_y^2+S_z^2}\right]$ $\frac{\tilde{\beta}}{\beta} = \frac{7\sqrt{3}}{6}\frac{r N_\lambda^S}{\pi p}\arcsin\left[\frac{p}{r}\frac{6}{7\sqrt{3}}\sqrt{S_x^2+S_y^2+S_z^2}\right]$
	TE-DRP-2-2-2-4-SG	$\frac{\tilde{\alpha}}{\alpha} = \frac{7.2192\sqrt{3}}{6}\frac{r N_\lambda^S}{\pi p}\arcsin\left[p\frac{6}{7.2192\sqrt{3}}\sqrt{S_{ox}^2+S_{oy}^2+S_{oz}^2}\right]$ $\frac{\tilde{\beta}}{\beta} = \frac{7.2192\sqrt{3}}{6}\frac{r N_\lambda^S}{\pi p}\arcsin\left[\frac{p}{r}\frac{6}{7.2192\sqrt{3}}\sqrt{S_{ox}^2+S_{oy}^2+S_{oz}^2}\right]$

$$N_\lambda = \frac{\lambda}{h} \qquad N_\lambda^S = \frac{\lambda_S}{h} \qquad r = \frac{\alpha}{\beta} \qquad kh = \frac{2\pi}{N_\lambda}$$

P-wave:

$$k_x h = \frac{2\pi}{r N_\lambda^S}\cos\varphi\sin\delta \;,\; k_y h = \frac{2\pi}{r N_\lambda^S}\sin\varphi\sin\delta \;,\; k_z h = \frac{2\pi}{r N_\lambda^S}\cos\delta$$

S-wave:

$$k_x h = \frac{2\pi}{N_\lambda^S}\cos\varphi\sin\delta \;,\; k_y h = \frac{2\pi}{N_\lambda^S}\sin\varphi\sin\delta \;,\; k_z h = \frac{2\pi}{N_\lambda^S}\cos\delta$$

Figure 14. Relations for the normalized grid phase velocities for the two FD schemes in 1-D and 3-D. Here, $\tilde{c}$ and c are the grid and true phase velocities in 1-D, $\tilde{\alpha}$ and α are the grid and true phase velocities in 3-D, $\tilde{\beta}$ and β are the grid and true phase velocities in 3-D, N_λ is the spatial sampling in 1-D, N_λ^S is spatial sampling of the *S*-wave in 3-D, r is the *P*-wave to *S*-wave speed ratio, δ is angle between the positive z axis and wavenumber vector $\vec{k}$(the direction of propagation), φ is angle between the positive x axis and the vertical plane determined by the z axis and wavenumber vector $\vec{k}$. The meaning of other quantities is the same as in Fig. 13.

7 NUMERICAL COMPARISON OF SCHEMES

The derived FD schemes may be compared in different ways. The basic comparisons assume propagation of a harmonic plane wave in an unbounded homogeneous medium. The most usual way is to compare stability and grid dispersion. In the analysis of grid dispersion, we assume a constant amplitude of the grid wave (wave propagating in the stable non-attenuative regime). Complementary, we may also quantify how the exact amplitude changes in one time step due to inaccuracy of a numerical scheme. See, for example, Moczo *et al*. (2014) for more details.

Here, we also assume a plane-wave propagation in an unbounded homogeneous medium. However, in order to quantify the overall waveform accuracy in a broad frequency range we evaluate the sum of the phase and envelope misfits between the FD and exact solutions. In this way we integrally capture both the phase and envelope inaccuracies. As found out by extensive numerical testing and comparisons (Chaljub *et al*. 2010, 2015 and Maufroy *et al*. 2015), the sum of the phase and envelope misfits in a homogeneous medium better indicates accuracy in heterogeneous media—which is the most important criterion. After we find the best scheme(s), we will also analyse their stability and grid dispersion.

7.1 Misfit between the FD and exact seismograms

Thus, in order to compare accuracy of the 1-D FD schemes we numerically simulated propagation of a plane wave in an unbounded homogeneous elastic medium with wave speed of 3700 m s^{-1} and density 2800 kg m^{-3}. (In 1-D, we do not need to recognize the type of wave.) We simulated plane-wave radiation using the Alterman & Karal (1968) decomposition applied to the particle velocity. As a source-time function, we used a narrow delta-like signal with a broad amplitude spectrum. For an FD scheme, we used a uniform grid with a grid spacing h and time step Δt. We recorded a numerically simulated wave at a travel distance of 20 wavelengths at frequency 1 Hz. For the synthetic seismogram and the true solution, we calculated the frequency-dependent phase and envelope misfits (Kristeková *et al*. 2009). In other words, we obtained a value of the phase misfit and a value of the envelope misfit for each frequency. For each frequency, we divided the values of misfits by the corresponding frequency. The obtained (i.e. frequency-normalized) misfits thus represent for each frequency the phase and envelope misfits at the travel distance of 20 wavelengths corresponding to the respective frequency. The broad amplitude spectrum of the

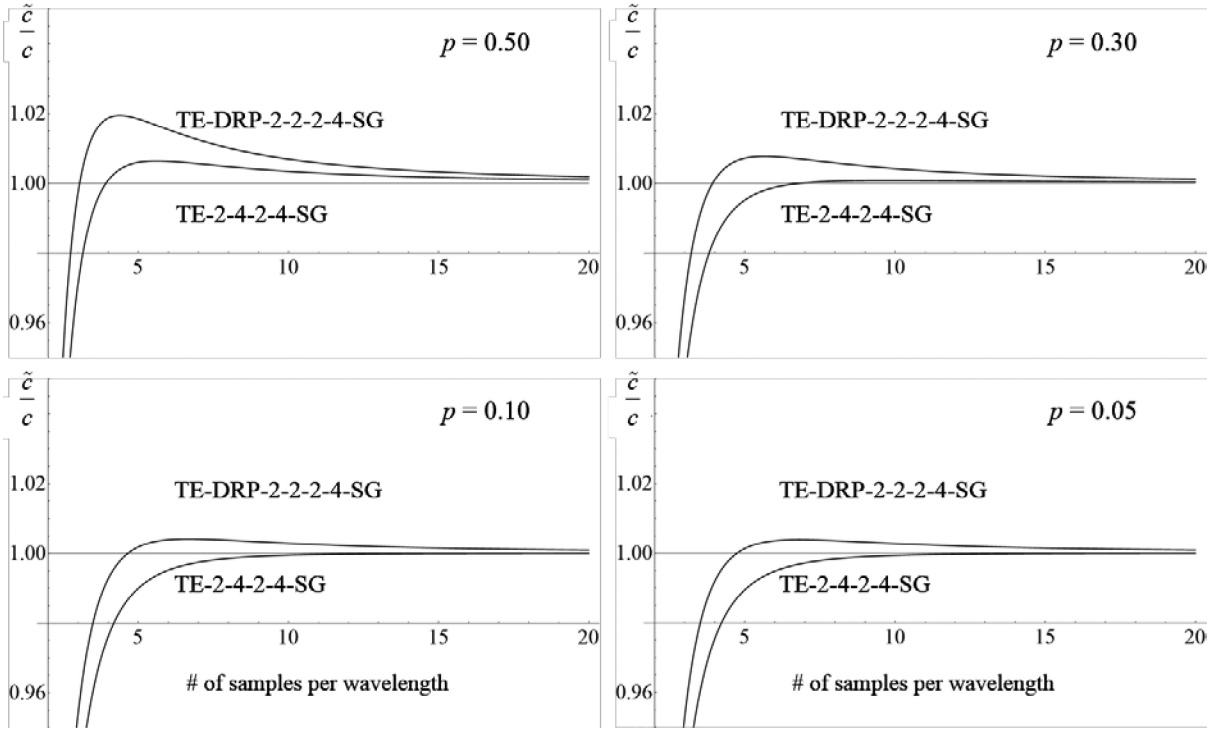

Figure 15. Normalized grid phase velocities for the TE-2-4-2-4-SG and TE-DRP-2-2-2-4-SG schemes in 1-D.

delta-like source-time function thus enabled us to evaluate misfits for spatial sampling (the number of grid spacings per wavelength) in the range of [2,50]. We calculated the misfits for different values of the stability ratio, that is, for different values of time step.

The general form of the stability condition for 1-D FD schemes can be written as $S = c\,\Delta t/h \leq S_M$ where S is known as Courant number. The stability ratio may be defined as $p \equiv \frac{c\,\Delta t}{h\,S_M}$. Then $\Delta t = p\,\frac{h}{c}\,S_M\,; \quad 0 < p \leq 1$. We have not analysed stability of all the 14 numerically investigated schemes and thus we do not know values of S_M which may be slightly different for different schemes. For a unified treatment, we assume $S_M = 1$ and consequently $\Delta t = p\,h/c$ which means that h/c is considered as the maximum possible time step for all investigated schemes. In Figs 11 and 12, we show the sum of the envelope misfit (EM) and phase misfit (PM) as a function of the number of grid spacings per wavelength for three values of the stability ratio: $p \in \{0.05,\ 0.3,\ 0.5\}$. For example, $p = 0.5$ means that we consider half of the maximum possible time step.

In Fig. 11, we show the misfits in the range of [0,70] per cent in order to have a global overview of the all investigated schemes. We can distinguish three groups of the misfit curves:

(1) DRP-0-0-3-5-CG, DRP-0-0-3-7-CG (black dashed and dash-dot misfit curves)
(2) DRP-0-0-2-4-SG, TE-DRP-0-2-2-4-SG (black and brown solid misfit curves)
(3) TE-2-4-3-5-CG, TE-2-4-3-7-CG, TE-DRP-2-2-3-5-CG, TE-DRP-2-2-3-7-CG, TE-2-2-2-2-SG, TE-2-4-2-4-SG, TE-DRP-2-2-2-4-SG

In Fig. 11, we show only 12 of 14 FD schemes listed in Section 6. We do not include the two simplest CG schemes—TE-2-2-3-3-CG = DRP-0-0-3-3-CG. This is because these schemes split (odd-even decoupling) into two non-communicating SG schemes with grid spacing $2h$.

Any of the DRP or TE-DRP schemes with 0th-order accuracy in time and/or space (misfit curves in the first and second groups) is too much inaccurate and thus practically unusable. We will not consider them further. We can also see that schemes TE-DRP-2-2-2-4-SG (red solid) and TE-2-4-2-4-SG (blue solid) have relatively small misfits in the broadest frequency range—as compared with all other investigated schemes.

In order to better compare schemes in the range of relatively small misfits, Fig. 12 shows the misfit curves in the range of [0,6] per cent. This relatively detailed view on the misfit curves better visualizes what we could notice in Fig. 11: the standard (2,4) staggered-grid scheme, TE-2-4-2-4-SG (blue solid), and TE-DRP optimized scheme TE-DRP-2-2-2-4-SG (red solid) have the smallest misfit values at low spatial sampling. Their mutual comparison is, however, not simple. Whereas TE-2-4-2-4-SG (blue solid) is clearly better for $p = 0.5$, TE-DRP-2-2-2-4-SG (red solid) has smaller misfit for less than 8 grid spacings per wavelength if $p = 0.05$. If $p = 0.3$, TE-DRP-2-2-2-4-SG (red solid) has smaller misfit for less than 5 grid spacings per wavelength, whereas TE-2-4-2-4-SG (blue solid) is better for more than 6 grid spacings per wavelength. Consequently, we should properly interpret these comparisons with respect to heterogeneity of the medium.

In a homogeneous medium, we should use the maximum possible time step or, rigorously said, the maximum possible fraction of the theoretically maximal time step according to the stability condition. In our case, choice $p = 0.5$ corresponds the most to such requirement. We can see that from the all investigated schemes the standard SG scheme, TE-2-4-2-4-SG, is the best scheme.

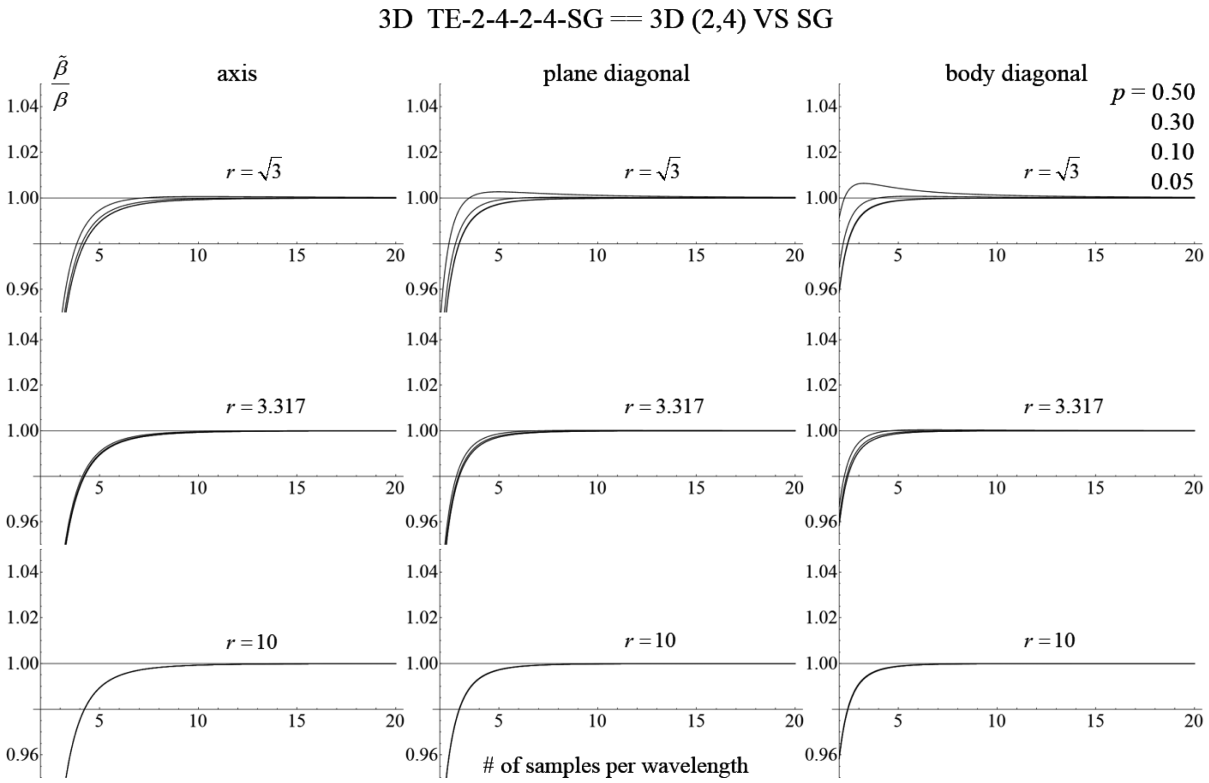

Figure 16. The 3-D TE-2-4-2-4-SG normalized grid phase velocity of the plane *S* wave propagating in the three distinct directions: along a coordinate axis ($\delta = 90°,\ \varphi = 0°$), coordinate-plane diagonal ($\delta = 45°,\ \varphi = 0°$) and body diagonal ($\delta = 54.74°,\ \varphi = 45°$). The dispersion curves are shown for four values of the stability ratio p and three values of the *P*-wave to *S*-wave speed ratio ($\sqrt{3},\ 3.317,\ 10$) corresponding to values 0.25, 0.45 and 0.495 of Poisson's ratio.

Consider 1-D modelling of *S* waves in a heterogeneous medium with a possibly large ratio between the minimum and maximum speeds. For example, in models with surface sediments the ratio between the *S*-wave speeds in underlying rock and surface sediments, say VS_R/VS_S, is often between 2 and 10. For a fixed value of the grid spacing h, the maximum possible time step Δt is given by the stability condition $S \leq S_M$ determined by the VS_R. Courant number S for the sediments is, however, VS_R/VS_S smaller than Courant number for the underlying rock. Consequently, the time step applied to sediments is VS_R/VS_S smaller than that required by the stability condition only for sediments. This means that if $p = 0.5$ in the rock beneath sediments, $p = 0.5\ VS_S/VS_R$ in sediments. Curves for $p = 0.3$ and $p = 0.05$ thus possibly correspond to situations in sediments (assuming one grid spacing h and one time step Δt for the whole model and grid).

In 2-D and 3-D modelling, p in sediments may be even smaller because Δt is determined by VP_R, and consequently p in sediments is proportional to VS_S/VP_R.

Clearly, in practical simulations we should adjust the choice of a FD scheme according to the model. In a model in which the actual value of the stability ratio in sediments is considerably smaller than that in the underlying rock, we should use TE-DRP-2-2-2-4-SG if we do not want to use considerably denser spatial sampling than it is usual. Recall that in numerical modelling of earthquake ground motion using the (2,4) staggered-grid FD scheme (that is TE-2-4-2-4-SG) modellers usually apply six grid spacings per wavelength.

The very important practical aspect of using scheme TE-DRP-2-2-2-4-SG in comparison with scheme TE-2-4-2-4-SG is that they differ from each other only in values of coefficients—see schemes (C10) and (C14) in Appendix C. In other words, in the computer codes based on scheme TE-2-4-2-4-SG it is enough to redefine the values of the approximation coefficients.

Let us briefly comment on the five other schemes for which misfits are shown in Fig. 12. The third of the SG schemes, the second-order in space and time TE-2-2-2-2-SG is shown mainly for comparison with TE-2-4-2-4-SG and TE-DRP-2-2-2-4-SG. As expected, this is the least accurate of the three SG schemes and practically unusable. It is therefore interesting to see this SG scheme among the four CG schemes. The accuracy of the four CG schemes is relatively low. Neither the mutual comparison of the four schemes nor explanation of the misfit curves of the individual schemes is easy. Recall that the simplest CG scheme TE-2-2-3-3-CG (=DRP-0-0-3-3-CG) splits (odd-even decoupling) into two non-communicating SG schemes with grid spacing $2h$. The four CG schemes in Fig. 12 differ from the simplest CG scheme only by a few more grid points. Probably these additional points add only little-weighted values to the simplest scheme and therefore they cannot be sufficiently accurate.

7.2 Stability and grid dispersion of the TE-2-4-2-4-SG and TE-DRP-2-2-2-4-SG schemes

Stability and grid dispersion of the standard TE-2-4-2-4-SG are well known. Here we compare the stability and grid dispersion in a concise way. The dispersion relations and the consequent stability conditions for both the 1-D and 3-D schemes are summarized in Fig. 13. As we

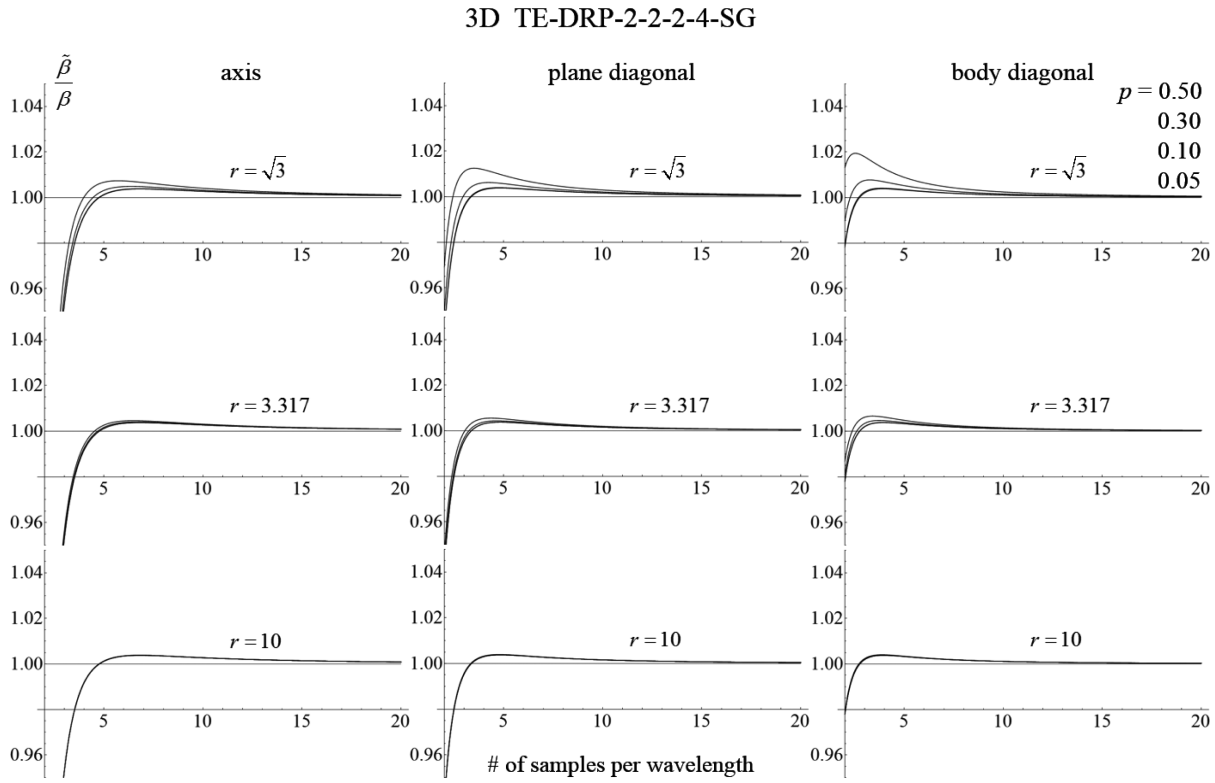

Figure 17. The same as in Fig. 16 but for the 3-D TE-DRP-2-2-2-4-SG scheme.

could expect, the maximum Courant numbers for the two schemes only slightly differ. Fig. 14 summarizes the corresponding relations for the normalized grid phase velocities. Note that we use symbols α and β for conciseness in Figs 13 and 14 instead of V_P and V_S for the *P*-wave and *S*-wave speeds and velocities.

In Fig. 15, we show normalized grid phase velocities for the two 1-D schemes for four values of the stability ratio: $p \in \{0.5,\ 0.3,\ 0.1,\ 0.05\}$ assuming $S_M = 1$ for both schemes. The reason is consistency with the investigation in terms of the phase and envelope misfit in Section 7.1. The assumption means that the true time steps corresponding to $p \in \{0.5,\ 0.3,\ 0.1,\ 0.05\}$ are 7/6 and 7.1912/6, respectively, times larger fractions of the maximum possible time steps for the two schemes. The dispersion curves are qualitatively consistent with the previous observations based on evaluation of the misfits: for small fractions of the maximum time steps, the TE-DRP-2-2-2-4-SG grid velocities are for smaller values of the spatial sampling closer to the true velocities than the TE-2-4-2-4-SG grid velocities are.

In Figs 16 and 17, we show the normalized grid *S*-wave phase velocities for the TE-2-4-2-4-SG and TE-DRP-2-2-2-4-SG schemes in 3-D, respectively. The figures show velocities for three directions of propagations—along a coordinate axis, plane diagonal and body diagonal—for three values of the *P*-wave to *S*-wave speed ratio. The three values correspond to values 0.25, 0.45 and 0.495 of Poisson's ratio. The comparison for the 1-D schemes is also true for the 3-D schemes.

7.3 Comparison with the spectral-element solution for a 3-D Mygdonian basin model

Here we present an illustrative numerical example for a complex 3-D model of the Mygdonian basin near Thessaloniki, Greece. Detailed descriptions of the model and numerical simulations are given in the article by Kristek *et al*. (2016). Here, we only briefly show the geometry and material parameters—Figs 18 and 19.

The wavefield is generated by a double-couple point source located at a depth of 5 km. The source-time function is defined as a low-pass filtered Gaussian pulse.

The reference spectral-element (SEM) seismograms were computed by Emmanuel Chaljub using the SPECFEM3D code developed by Komatitsch and Tromp (e.g. Komatitsch & Tromp 1999; Tromp *et al*. 2008; Peter *et al*. 2011). In the computational model, geometry of material interfaces was modified so that the element faces can exactly follow interfaces. This implies that the SEM simulation exactly accounts for the geometry of material interfaces and consequently the SEM seismograms can be considered a reference. The FDM seismograms were computed using the FDSim3D code (Kristek & Moczo 2014; Moczo *et al*. 2014). Fig. 20 shows three curves of the envelope and phase GOFs (goodness-of-fit) between the reference SEM seismograms and FDM seismograms along the western, central and eastern receiver profiles. Each curve represents GOF between the SEM and one of the three FD solutions. GOFs are calculated for the entire 30-s window in the frequency range [0.1, 5] Hz from the arithmetic average of the single-valued misfits evaluated separately for each component (Kristeková

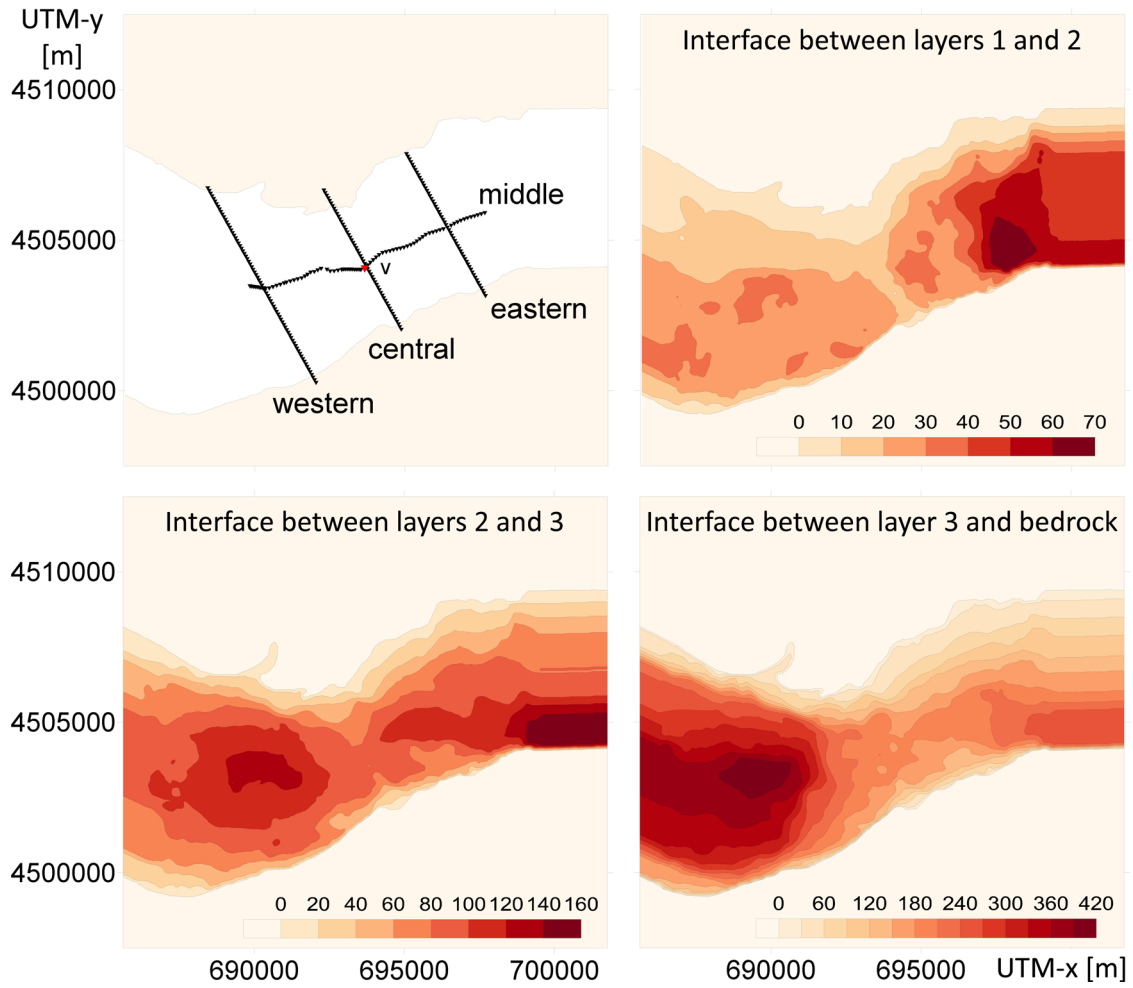

Figure 18. Geometry of the original 3-D model of the Mygdonian basin. Upper left panel: margins of the sedimentary basin at the flat free surface, four horizontal profiles of receivers at the free surface and position of the vertical profile of receivers (v) in the central part of the basin. Upper right: interface between the uppermost and middle sedimentary layers. Lower left: interface between the middle and bottom sedimentary layers. Lower right: interface between the bottom sedimentary layer and bedrock.

Layer	V_S	V_P	ρ
	(m/s)	(m/s)	(kg/m^3)
1	200	1500	2100
2	350	1800	2200
3	650	2500	2200
Bedrock	2600	4500	2600

Figure 19. Material parameters of the 3-D model of the Mygdonian basin.

et al. 2009). Fig. 21 shows the envelope and phase GOFs for the middle and vertical receiver profiles. Recall that GOF = 10 means the perfect agreement. The seismograms obtained using the 3-D TE-2-4-2-4-SG scheme with a 7 m grid spacing are in a very good agreement with the reference SEM seismograms. We can see that with a coarser 10 m grid spacing the better result, in terms of the phase GOFs, is obtained using the 3-D TE-DRP-2-2-2-4-SG scheme. Though the envelope GOF is not improved, improvement in the phase GOF is considerable. In other wavefields, it is possible that both the envelope and phase GOFs can be improved due to application of the TE-DRP-2-2-2-4-SG scheme. The main aspect of this is that a possible improvement does not require any additional computational load.

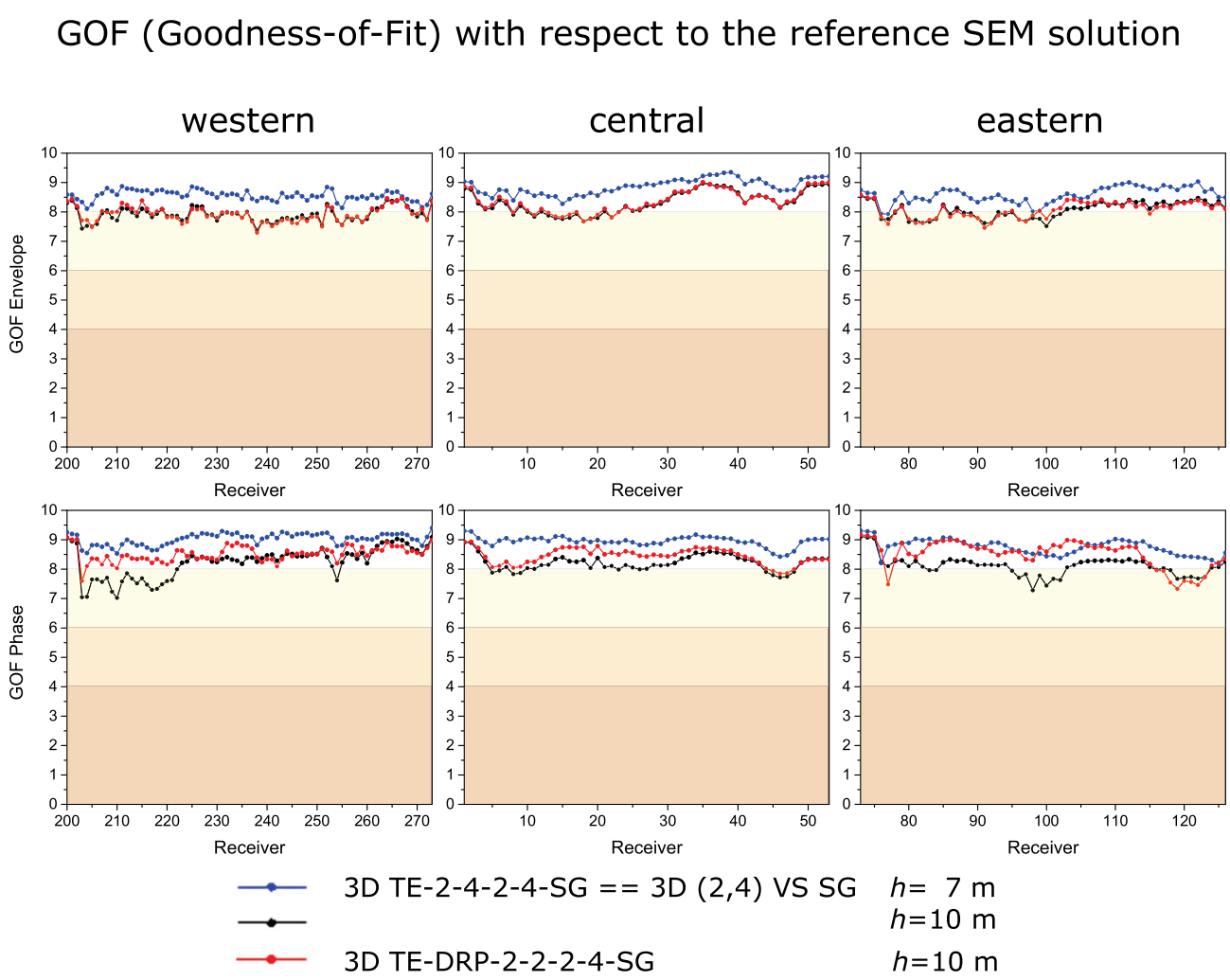

Figure 20. The envelope and phase GOFs (goodness-of-fit) between the reference SEM seismograms and three FDM seismograms along the western, central and eastern receiver profiles. (Note that GOF = 10 means the perfect agreement.)

8 CONCLUSIONS

We addressed the problem of the FD approximations of the VS formulation of the equation of motion and constitutive law on two fundamental types of grids: SG and CG. In a general 3-D problem, the two grids may be considered extreme cases (in terms of distribution of field variables and approximation of derivatives) of the set of four grids—staggered, partly staggered, Lebedev and collocated. In a 1-D problem, the staggered, partly staggered and Lebedev grids coincide.

For approximating the first spatial and temporal derivatives, we used three approaches—TE, DRP, and combined TE-DRP. The TE and DRP criterion represents two fundamental extreme approaches. In the TE approach, the spatial and temporal derivatives are approximated in the same formal mathematical way using truncated TE. Quality or accuracy of approximation is quantified by the order of truncation. In the DRP approach, approximation of the spatial derivative is based on minimization of difference between true and numerical wavenumbers. Approximation of the temporal derivative is based on minimization of difference between true and numerical frequencies. In the TE sense, the DRP approximations are 0th-order accurate. The combined TE-DRP approach gives an approximation with order of accuracy larger than zero and partial application of the DRP criterion.

In this article we

(1) derived original useful formulae for the DRP and TE-DRP approximations of the spatial and temporal derivatives on the SG and CG,
(2) analysed accuracy of the numerical wavenumbers and numerical frequencies of the basic TE, DRP and TE-DRP approximations,
(3) applied the approximations for finding 3 TE, 3 DRP and 2 TE-DRP basic FD schemes on the CG,
(4) applied the approximations for finding 2 TE, 2 DRP and 2 TE-DRP basic FD schemes on the SG,
(5) performed systematic numerical comparison of the 14 FD schemes in a homogeneous medium,
(6) analysed stability and grid dispersion of the two best schemes in 1-D and 3-D,
(7) performed 3-D numerical tests.

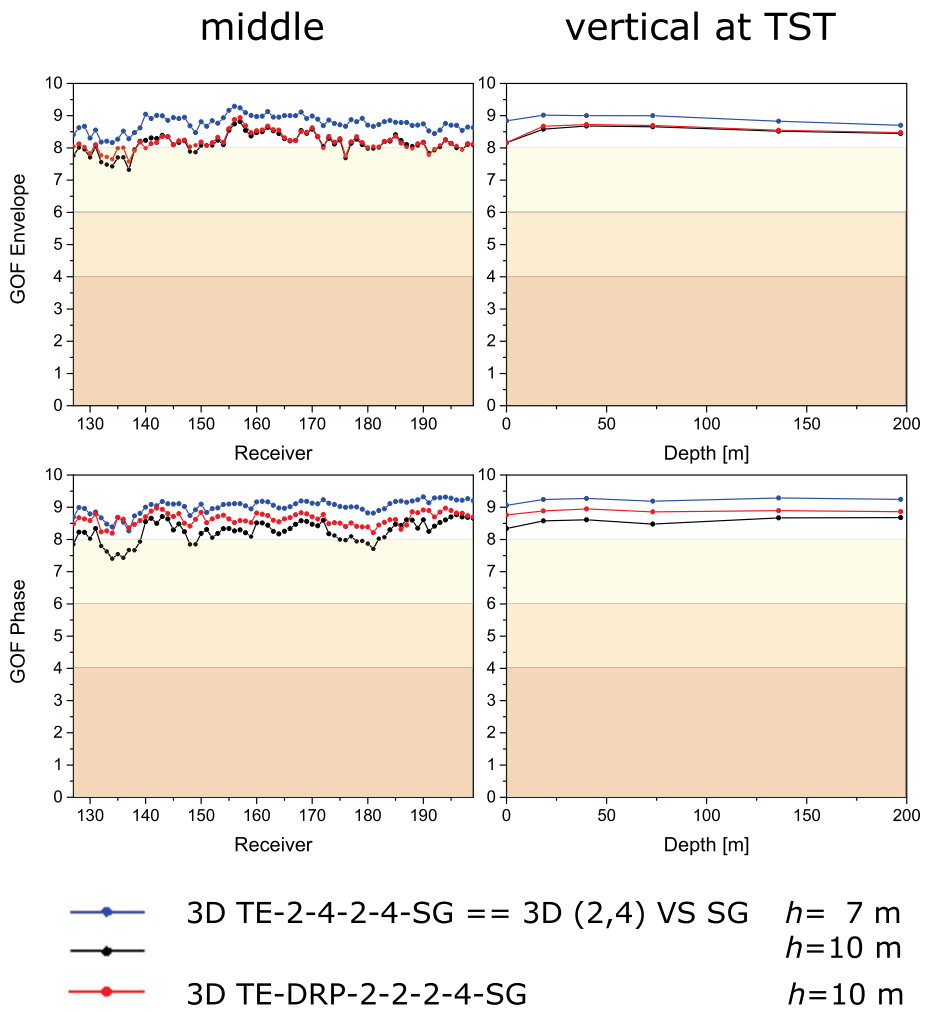

Figure 21. The envelope and phase GOFs (goodness-of-fit) between the reference SEM seismograms and three FDM seismograms along the middle and vertical receiver profiles.

We have found that

(1) for a fixed number of grid points the use of the DRP criterion, as compared to the TE approach, increases the acceptable range of $k\Delta x$ in approximating the spatial derivative on both the SG and CG,

(2) for a fixed number of time levels the use of the DRP criterion, as compared to the TE approach, increases the acceptable range of $\omega\,\Delta t$ in approximating the temporal derivative on both the SG and CG,

(3) the use of the SG, as compared to the CG, increases acceptable range of $k\Delta x$ in approximating the spatial derivative,

(4) the use of the staggered-grid, as compared to the collocated-grid, increases acceptable range of $\omega\,\Delta t$ in approximating the temporal derivative,

(5) TE-2-4-2-4-SG scheme, that is, TE second-order in time, TE fourth-order in space, 2-point in time ($M_{\mathrm{Time}} = -N_{\mathrm{Time}} = 1/2$), 4-point in space ($M_{\mathrm{Space}} = -N_{\mathrm{Space}} = 3/2$) is the best scheme for large fractions of the maximum possible time step, or, in other words, in a homogeneous medium,

(6) TE-DRP-2-2-2-4-SG scheme, that is, TE second-order in time, combined TE-DRP second-order in space, 2-point in time ($M_{\mathrm{Time}} = -N_{\mathrm{Time}} = 1/2$), 4-point in space ($M_{\mathrm{Space}} = -N_{\mathrm{Space}} = 3/2$) with $a_{-1/2}$ and $a_{1/2}$ being free parameters, is the best scheme for small fractions of the maximum possible time step, or, in other words, in models with large velocity contrasts if uniform spatial grid spacing and time step are used.

In practical simulations, we should adjust the choice of a FD scheme to a model. In a model in which the actual value of the stability ratio in sediments is considerably smaller than that in the underlying rock, we should use TE-DRP-2-2-2-4-SG if we do not want to use considerably denser spatial sampling than it is usual (in numerical modelling of earthquake ground motion using the (2,4) staggered-grid FD scheme, that is TE-2-4-2-4-SG, modellers usually apply 6 grid spacings per wavelength). TE-DRP-2-2-2-4-SG differs from TE-2-4-2-4-SG only in values of coefficients. This means, that in computer codes based on scheme TE-2-4-2-4-SG it is enough to redefine the values of the approximation coefficients.

ACKNOWLEDGEMENTS

This work was supported in part by the Slovak Research and Development Agency under the contracts APVV-0271-11 (project MYGDONEMOTION) and project SIGMA (EDF, AREVA, CEA and ENEL). We thank Josep de la Puente for his valuable comments and suggestions that helped to improve the article.

REFERENCES

Alterman, Z.S. & Karal, F.C., 1968. Propagation of elastic waves in layered media by finite difference methods, *Bull. seism. Soc. Am.,* **58**(1), 367–398.

Andrews, D.J., 1973. A numerical study of tectonic stress release by underground explosions, *Bull. seism. Soc. Am.,* **63**(4), 1375–1391.

Bayliss, A., Jordan, K.E., LeMesurier, B.J. & Turkel, E., 1986. A fourth-order accurate finite-difference scheme for the computation of elastic waves, *Bull. seism. Soc. Am.,* **76**(4), 1115–1132.

Blanch, J.O. & Robertsson, J.O.A., 1997. A modified Lax-Wendroff correction for wave propagation in media described by Zener elements, *Geophys. J. Int.,* **131,** 381–386.

Chaljub, E., Moczo, P., Tsuno, S., Bard, P.-Y., Kristek, J., Käser, M., Stupazzini, M. & Kristekova, M., 2010. Quantitative comparison of four numerical predictions of 3D ground motion in the Grenoble valley, France, *Bull. seism. Soc. Am.,* **100**(4), 1427–1455.

Chaljub, E. *et al.*, 2015. 3-D numerical simulations of earthquake ground motion in sedimentary basins: testing accuracy through stringent models, *Geophys. J. Int.,* **201**(1), 90–111.

Chen, H., Zhou, H., Zhang, Q. & Zhang, Q., 2015. Optimized time-space domain staggered-grid finite-difference methods based on new finite-difference stencils, in *SEG Technical Program Expanded Abstracts* 2015, pp. 3672–3676.

Geller, R.J. & Takeuchi, N., 1995. A new method for computing highly accurate DSM synthetic seismograms, *Geophys. J. Int.,* **123,** 449–470.

Geller, R.J. & Takeuchi, N., 1998. Optimally accurate second-order time-domain finite difference scheme for the elastic equation of motion: one-dimensional cases, *Geophys. J. Int.,* **135,** 48–62.

Hixon, R., 1997. On increasing the accuracy of MacCormack schemes for aeroacoustic applications, in *Proceedings of the 3rd AIAA/CEAS Aeroacoustics Conference*, Atlanta, GA, pp. 29–39. AIAA Paper 97–1586.

Holberg, O., 1987. Computational aspects of the choice of operator and sampling interval for numerical differentiation in large-scale simulation of wave phenomena, *Geophys. Prospect.,* **35,** 629–655.

Hu, F.Q., Hussaini, M.Y. & Manthey, J.L., 1996. Low-Dissipation and Low-Dispersion Runge–Kutta Schemes for Computational Acoustics, *J. Comput. Phys.,* **124,** 177–191.

Kindelan, M., Kamel, A. & Sguazzero, P., 1990. On the construction and efficiency of staggered numerical differentiators for the wave equation, *Geophysics,* **55,** 107–110.

Komatitsch, D. & Tromp, J., 1999. Introduction to the spectral-element method for 3-D seismic wave propagation, *Geophys. J. Int.,* **139**(3), 806–822.

Kristek, J. & Moczo, P., 2014. FDSim3D - The Fortran95 Code for Numerical Simulation of Seismic Wave Propagation in 3D Heterogeneous Viscoelastic Media. www.cambridge.org/moczo.

Kristek, J., Moczo, P., Chaljub, E. & Kristeková, M. 2016. An orthorhombic representation of a heterogeneous medium for the finite-difference modelling of seismic wave propagation, *Geophys. J. Int.*, submitted.

Kristeková, M., Kristek, J. & Moczo, P., 2009. Time-frequency misfit and goodness-of-fit criteria for quantitative comparison of time signals, *Geophys. J. Int.,* **178,** 813–825.

Lax, P. & Wendroff, B., 1960. Systems of conservation laws, *Commun. Pure appl. Math.,* **13,** 217–237.

Lebedev, V.I., 1964. Difference analogues of orthogonal decompositions of basic differential operators and some boundary value problems. I., *Zh. Vychisl. Mat. Mat. Fiz.,* **4,** 449–465 (in Russian).

Levander, A.R., 1988. Fourth-order finite-difference *P-SV* seismograms, *Geophysics,* **53,** 1425–1436.

Liang, W., Wang, Y. & Yang, C., 2015. Determining finite difference weights for the acoustic wave equation by a new dispersion-relationship-preserving method, *Geophys. Prospect.,* **63,** 11–22.

Lisitsa, V., 2007. Lebedev scheme for anisotropic elastic problems, in *Proceedings of 8th International Conference on Theoretical and Computational Acoustics*, pp. 331–341, doi:10.3997/2214-4609.201401952.

Lisitsa, V. & Vishnevskiy, D., 2010. Lebedev scheme for the numerical simulation of wave propagation in 3D anisotropic elasticity, *Geophys. Prospect.,* **58,** 619–635.

MacCormack, R.W., 1969. The effect of viscosity in hypervelocity impact cratering, AIAA Paper 69-354.

MacCormack, R.W., 1971. Numerical solution of the interaction of a shock wave with a laminar boundary layer, in *Proc. of the Second Intl. Conference on Numerical Methods in Fluid Dynamics*, Lecture notes in physics, Springer-Verlag, New York, pp. 151–163.

Madariaga, R., 1976. Dynamics of an expanding circular fault, *Bull. seism. Soc. Am.,* **66,** 639–666.

Maufroy, E. *et al.*, 2015. Earthquake ground motion in the Mygdonian basin, Greece: The E2VP verification and validation of 3D numerical simulation up to 4 Hz, *Bull. seism. Soc. Am.,* **105**(3), 1398–1418.

Moczo, P., Kristek, J. & Bystrický, E., 2001. Efficiency and optimization of the 3-D finite-difference modeling of seismic ground motion, *J. Comput. Acoust.,* **9,** 593–609.

Moczo, P., Kristek, J. & Gális, M., 2014. *The Finite-Difference Modelling of Earthquake Motions: Waves and Ruptures*, Cambridge Univ. Press.

Peter, D. *et al.*, 2011. Forward and adjoint simulations of seismic wave propagation on fully unstructured hexahedral meshes, *Geophys. J. Int.,* **186**(2), 721–739.

Robertsson, J.O.A., Blanch, J.O., Nihei, K. & Tromp, J., 2012. *Numerical Modeling of Seismic Wave Propagation: Gridded Two-Way Wave-Equation Methods*, *Geophysical Reprint Series* No. 28, Society of Exploration Geophysicists.

Saenger, E.H., Gold, N. & Shapiro, S.A., 2000. Modeling the propagation of elastic waves using a modified finite-difference grid, *Wave Motion,* **31,** 77–92.

Song, X., Fomel, S. & Ying, L., 2013. Lowrank finite-differences and lowrank Fourier finite-differences for seismic wave extrapolation in the acoustic approximation, *Geophys. J. Int.,* **193,** 960–969.

Tabei, M., Mast, T.D. & Waag, R.C., 2002. A k-space method for coupled first-order acoustic propagation equations, *J. acoust. Soc. Am.,* **111,** 53–63.

Tam, C.K.W. & Webb, J.C., 1993. Dispersion-relation-preserving finite difference schemes for computational acoustics, *J. Comput. Phys.,* **107,** 262–281.

Tan, S. & Huang, L., 2014. An efficient finite-difference method with high-order accuracy in both time and space domains for modelling scalar-wave propagation, *Geophys. J. Int.,* **197,** 1250–1267.

Tromp, J., Komatitsch, D. & Liu, Q., 2008. Spectral-element and adjoint methods in seismology, *Commun. Comput. Phys.,* **3**(1), 1–32.

Virieux, J., 1984. *SH*-wave propagation in heterogeneous media: velocity-stress finite-difference method, *Geophysics,* **49,** 1933–1957.

Virieux, J., 1986. *P-SV* wave propagation in heterogeneous media: velocity-stress finite-difference method, *Geophysics,* **51,** 889–901.

Zhang, W. & Chen, X., 2006. Traction image method for irregular free surface boundaries in finite difference seismic wave simulation, *Geophys. J. Int.,* **167,** 337–353.

Zhang, W., Zhang, Z. & Chen, X., 2012. Three-dimensional elastic wave numerical modelling in the presence of surface topography by a collocated-grid finite-difference method on curvilinear grids, *Geophys. J. Int.,* **190,** 358–378.

APPENDIX A

An example of calculation of coefficients using the TE-DRP combination for approximating a spatial derivative on the collocated grid:

Recall eq. (4):

$$\frac{\partial f}{\partial x}(x) \approx \frac{1}{\Delta x}\sum_{j=N}^{M} a_j\, f\,(x + j\Delta x). \tag{A1}$$

Consider $N = -2$, $M = 3$, and a_{-2} and a_2 as free parameters. This means that eq. (6) should be satisfied for $r = 0, \ldots, 3$. Consequently, approximation (4) is accurate up to order $(\Delta x)^3$. According to eq. (6)

$$\sum_{j=-2}^{3} j^r a_j = \delta_{1r} \quad r = 0, \ldots, 3, \tag{A2}$$

that is,

$$\begin{aligned}
&(-2)^0 a_{-2} + (-1)^0 a_{-1} + (0)^0 a_0 + (1)^0 a_1 + (2)^0 a_2 + (3)^0 a_3 = 0\\
&(-2)^1 a_{-2} + (-1)^1 a_{-1} + (0)^1 a_0 + (1)^1 a_1 + (2)^1 a_2 + (3)^1 a_3 = 1\\
&(-2)^2 a_{-2} + (-1)^2 a_{-1} + (0)^2 a_0 + (1)^2 a_1 + (2)^2 a_2 + (3)^2 a_3 = 0\\
&(-2)^3 a_{-2} + (-1)^3 a_{-1} + (0)^3 a_0 + (1)^3 a_1 + (2)^3 a_2 + (3)^3 a_3 = 0.
\end{aligned} \tag{A3}$$

The two free parameters have the role to minimize error (10) in order to make the numerical and true wavenumbers as close as possible. Therefore, two equations should be satisfied according to eq. (16)

$$\sum_{j=-2}^{3} G_{sj} a_j = d_s \ , s = -2,\ 2. \tag{A4}$$

That is,

$$\begin{aligned}
&G_{-2,-2}a_{-2} + G_{-2,-1}a_{-1} + G_{-2,0}a_0 + G_{-2,1}a_1 + G_{-2,2}a_2 + G_{-2,3}a_3 = d_{-2},\\
&G_{2,-2}a_{-2} + G_{2,-1}a_{-1} + G_{2,0}a_0 + G_{2,1}a_1 + G_{2,2}a_2 + G_{2,3}a_3 = d_2.
\end{aligned} \tag{A5}$$

Coefficients G_{sj} are calculated according to eq. (17). Combination of eqs (A3) and (A5) gives a system of linear equations for calculating unknown coefficients a_j.

APPENDIX B

Using two alternative approaches for approximating temporal derivative on the collocated grid

Consider, for example, equation

$$\frac{\partial f}{\partial t} = c\frac{\partial f}{\partial x}. \tag{B1}$$

Recall eqs (21) and (23) for approximating temporal derivatives with two alternative approaches, respectively:

$$f\,(t + \Delta t) - f\,(t) \approx \Delta t \sum_{j=0}^{M} \beta_j \frac{\partial f}{\partial t}\,(t - j\Delta t) \tag{B2}$$

and

$$\frac{\partial f}{\partial t}(t) \approx \frac{1}{\Delta t}\sum_{j=N}^{M=1} b_j\, f(t + j\Delta t). \tag{B3}$$

Recall eq. (4) for approximating spatial derivatives

$$\frac{\partial f}{\partial x}(x) \approx \frac{1}{\Delta x}\sum_{j=N}^{M} a_j\, f\,(x + j\Delta x). \tag{B4}$$

Approximate eq. (B1) with the first approach. Define

$$L(t, x) \equiv \frac{\partial f}{\partial t}(t, x). \tag{B5}$$

Use definition (B5) and approximate the spatial derivative on the r.h.s. of eq. (B1) using eq. (B4):

$$L(t,x) = \frac{c}{\Delta x} \sum_{j=N_{\text{Space}}}^{M_{\text{Space}}} a_j \, f(t, x + j\Delta x). \tag{B6}$$

Applying eq. (B2) in (B5) we obtain

$$f(t + \Delta t, x) - f(t,x) = \Delta t \sum_{j=0}^{M_{\text{Time}}} \beta_j \, L(t - j\Delta t, x). \tag{B7}$$

Hence, by using the first approach of approximating temporal derivate, we can approximate eq. (B1) using eqs (B6) and (B7).

Application of the second approach for approximating temporal derivative, eq. (B3), and eq. (B4) for approximating spatial derivative to eq. (B1) leads to

$$\frac{1}{\Delta t} \sum_{j=N_{\text{Time}}}^{M_{\text{Time}}=1} b_j \, f(t + j\Delta t, x) = \frac{c}{\Delta x} \sum_{j=N_{\text{Space}}}^{M_{\text{Space}}} a_j \, f(t, x + j\Delta x) \tag{B8}$$

and eventually to

$$f(t + \Delta t, x) = \frac{c\,\Delta t}{b_1 \Delta x} \sum_{j=N_{\text{Space}}}^{M_{\text{Space}}} a_j \, f(t, x + j\Delta x) - \frac{1}{b_1} \sum_{j=N_{\text{Time}}}^{M_{\text{Time}}=0} b_j \, f(t + j\Delta t, x). \tag{B9}$$

APPENDIX C

$\gamma = \Delta t / \Delta x$, $B_I = 1/\rho_I$

TE-2-2-3-3-CG:

$$\begin{aligned} V_I^{m+1} &= V_I^{m-1} + B_I \, \gamma \left(-T_{I-1}^m + T_{I+1}^m\right) + 2\Delta t \; B_I F_I^m \\ T_I^{m+1} &= T_I^{m-1} + C_I \, \gamma \left(-V_{I-1}^m + V_{I+1}^m\right) \end{aligned} \tag{C1}$$

TE-2-4-3-5-CG:

$$\begin{aligned} V_I^{m+1} &= V_I^{m-1} + \frac{1}{6} B_I \, \gamma \left(T_{I-2}^m - 8\,T_{I-1}^m + 8\,T_{I+1}^m - T_{I+2}^m\right) + 2\Delta t \; B_I F_I^m \\ T_I^{m+1} &= T_I^{m-1} + \frac{1}{6} C_I \, \gamma \left(V_{I-2}^m - 8\,V_{I-1}^m + 8\,V_{I+1}^m - V_{I+2}^m\right) \end{aligned} \tag{C2}$$

TE-2-4-3-7-CG:

$$\begin{aligned} V_I^{m+1} &= V_I^{m-1} + \frac{1}{12} B_I \, \gamma \left(-T_{I-3}^m + 6T_{I-2}^m - 21\,T_{I-1}^m + 21\,T_{I+1}^m - 6\,T_{I+2}^m + T_{I+3}^m\right) + 2\Delta t \; B_I F_I^m \\ T_I^{m+1} &= T_I^{m-1} + \frac{1}{12} C_I \, \gamma \left(-V_{I-3}^m + 6\,V_{I-2}^m - 21\,V_{I-1}^m + 21\,V_{I+1}^m - 6\,V_{I+2}^m + V_{I+3}^m\right) \end{aligned} \tag{C3}$$

DRP-0-0-3-3-CG:

$$\begin{aligned} V_I^{m+1} &= V_I^{m-1} + B_I \, \gamma \left(-T_{I-1}^m + T_{I+1}^m\right) + \frac{\Delta t}{0.636620} \; B_I F_I^m \\ T_I^{m+1} &= T_I^{m-1} + C_I \, \gamma \left(-V_{I-1}^m + V_{I+1}^m\right) \end{aligned} \tag{C4}$$

DRP-0-0-3-5-CG:

$$\begin{aligned} V_I^{m+1} = V_I^{m-1} &+ \frac{B_I \, \gamma}{0.636620} \left(0.144474 T_{I-2}^m - 0.759253\,T_{I-1}^m \right. \\ &\left. + 0.759253\,T_{I+1}^m - 0.144474 T_{I+2}^m\right) + \frac{\Delta t \; B_I}{0.636620} F_I^m \\ T_I^{m+1} = T_I^{m-1} &+ \frac{C_I \, \gamma}{0.636620} \left(0.144474 V_{I-2}^m - 0.759253\,V_{I-1}^m \right. \\ &\left. + 0\,.759253\,V_{I+1}^m - 0.144474 V_{I+2}^m\right) \end{aligned} \tag{C5}$$

DRP-0-0-3-7-CG:

$$V_I^{m+1} = V_I^{m-1} + \frac{B_I\ \gamma}{0.636620}\left(-0.067833T_{I-3}^m + 0.260749T_{I-2}^m - 0.857950\ T_{I-1}^m \right.$$
$$\left. + 0.857950\ T_{I+1}^m - 0.260749\ T_{I+2}^m + 0.067833T_{I+3}^m\right) + \frac{\Delta t\ B_I}{0.636620}F_I^m$$
$$T_I^{m+1} = T_I^{m-1} + \frac{C_I\ \gamma}{0.636620}\left(-0.067833V_{I-3}^m + 0.260749\ V_{I-2}^m - 0.857950\ V_{I-1}^m \right.$$
$$\left. + 0.857950\ V_{I+1}^m - 0.260749\ V_{I+2}^m + 0.067833V_{I+3}^m\right) \tag{C6}$$

TE-DRP-2-2-3-5-CG:

$$V_I^{m+1} = V_I^{m-1} + 2B_I\ \gamma\left(0.118679T_{I-2}^m - 0.737357T_{I-1}^m \right.$$
$$\left. + 0.737357\ T_{I+1}^m - 0.118679T_{I+2}^m\right) + 2\Delta t\ B_I F_I^m$$
$$T_I^{m+1} = T_I^{m-1} + 2C_I\ \gamma\left(0.118679\ V_{I-2}^m - 0.737357\ V_{I-1}^m \right.$$
$$\left. + 0.737357\ V_{I+1}^m - 0.118679\ V_{I+2}^m\right) \tag{C7}$$

TE-DRP-2-2-3-7-CG:

$$V_I^{m+1} = V_I^{m-1} + 2B_I\ \gamma\left(-0.052707T_{I-3}^m + 0.256037T_{I-2}^m - 0.853950\ T_{I-1}^m \right.$$
$$\left. 0.853950\ T_{I+1}^m - 0.256037T_{I+2}^m + 0.052707T_{I+3}^m\right) + 2\Delta t\ B_I F_I^m$$
$$T_I^{m+1} = T_I^{m-1} + 2C_I\ \gamma\left(-0.052707T_{I-3}^m + 0.256037T_{I-2}^m - 0.853950\ T_{I-1}^m \right.$$
$$\left. 0.853950\ T_{I+1}^m - 0.256037T_{I+2}^m + 0.052707T_{I+3}^m\right) \tag{C8}$$

TE-2-2-2-2-SG

$$V_I^{m+\frac{1}{2}} = V_I^{m-\frac{1}{2}} + B_I\ \gamma\left(-T_{I-\frac{1}{2}}^m + T_{I+\frac{1}{2}}^m\right) + \Delta t\ B_I F_I^m$$
$$T_{I-\frac{1}{2}}^m = T_{I-\frac{1}{2}}^{m-1} + C_{I-\frac{1}{2}}\ \gamma\left(-V_{I-1}^{m-\frac{1}{2}} + V_I^{m-\frac{1}{2}}\right) \tag{C9}$$

TE-2-4-2-4-SG:

$$V_I^{m+\frac{1}{2}} = V_I^{m-\frac{1}{2}} + \frac{1}{24}B_I\ \gamma\left(T_{I-\frac{3}{2}}^m - 27\ T_{I-\frac{1}{2}}^m + 27\ T_{I+\frac{1}{2}}^m - T_{I+\frac{3}{2}}^m\right) + \Delta t\ B_I F_I^m$$
$$T_{I-\frac{1}{2}}^m = T_{I-\frac{1}{2}}^{m-1} + \frac{1}{24}C_{I-\frac{1}{2}}\ \gamma\left(V_{I-2}^{m-\frac{1}{2}} - 27\ V_{I-1}^{m-\frac{1}{2}} + 27\ V_I^{m-\frac{1}{2}} - V_{I+1}^{m-\frac{1}{2}}\right) \tag{C10}$$

DRP-0-0-2-2-SG

$$V_I^{m+\frac{1}{2}} = V_I^{m-\frac{1}{2}} + B_I\ \gamma\left(-T_{I-\frac{1}{2}}^m + T_{I+\frac{1}{2}}^m\right) + \frac{\Delta t\ B_I}{1.063401}F_I^m$$
$$T_{I-\frac{1}{2}}^m = T_{I-\frac{1}{2}}^{m-1} + C_{I-\frac{1}{2}}\ \gamma\left(-V_{I-1}^{m-\frac{1}{2}} + V_I^{m-\frac{1}{2}}\right) \tag{C11}$$

DRP-0-0-2-4-SG:

$$V_I^{m+\frac{1}{2}} = V_I^{m-\frac{1}{2}} + \frac{B_I\ \gamma}{1.063401}\left(0.056845T_{I-\frac{3}{2}}^m - 1.162990\ T_{I-\frac{1}{2}}^m \right.$$
$$\left. + 1.162990\ T_{I+\frac{1}{2}}^m - 0.056844T_{I+\frac{3}{2}}^m\right) + \frac{\Delta t\ B_I}{1.063401}F_I^m$$
$$T_{I-\frac{1}{2}}^m = T_{I-\frac{1}{2}}^{m-1} + \frac{C_{I-\frac{1}{2}}\ \gamma}{1.063401}\left(0.056845V_{I-2}^{m-\frac{1}{2}} - 1.162990\ V_{I-1}^{m-\frac{1}{2}} \right.$$
$$\left. + 1.162990\ V_I^{m-\frac{1}{2}} - 0.056844V_{I+1}^{m-\frac{1}{2}}\right) \tag{C12}$$

TE-DRP-0-2-2-4-SG

$$V_I^{m+\frac{1}{2}} = V_I^{m-\frac{1}{2}} + \frac{B_I\ \gamma}{1.063401}\left(0.050800\,T^m_{I-\frac{3}{2}} - 1.152400\,T^m_{I-\frac{1}{2}} + 1.152400\,T^m_{I+\frac{1}{2}} - 0.050800T^m_{I+\frac{3}{2}}\right) + \frac{\Delta t\ B_I}{1.063401}F_I^m$$

$$T^m_{I-\frac{1}{2}} = T^{m-1}_{I-\frac{1}{2}} + \frac{C_{I-\frac{1}{2}}\ \gamma}{1.063401}\left(0.050800V_{I-2}^{m-\frac{1}{2}} - 1.152400\ V_{I-1}^{m-\frac{1}{2}} + 1.152400\ V_I^{m-\frac{1}{2}} - 0.050800V_{I+1}^{m-\frac{1}{2}}\right) \tag{C13}$$

TE-DRP-2-2-2-4-SG

$$V_I^{m+\frac{1}{2}} = V_I^{m-\frac{1}{2}} + B_I\ \gamma\left(0.050800\,T^m_{I-\frac{3}{2}} - 1.152400\,T^m_{I-\frac{1}{2}} + 1.152400\,T^m_{I+\frac{1}{2}} - 0.050800T^m_{I+\frac{3}{2}}\right) + \Delta t\ B_I F_I^m$$

$$T^m_{I-\frac{1}{2}} = T^{m-1}_{I-\frac{1}{2}} + C_{I-\frac{1}{2}}\ \gamma\left(0.050800V_{I-2}^{m-\frac{1}{2}} - 1.152400\ V_{I-1}^{m-\frac{1}{2}} + 1.152400\ V_I^{m-\frac{1}{2}} - 0.050800V_{I+1}^{m-\frac{1}{2}}\right) \tag{C14}$$